Glacial–to–Interglacial Changes of the Ocean Circulation and Eolian Sediment Transport

Bernd J. Haupt, Dan Seidov, and Eric J. Barron

EMS Environment Institute, Pennsylvania State University, University Park, Pennsylvania

Glacial–to–interglacial climate transitions are characterized by distinct basin–wide sediment accumulation patterns that can reveal accompanying ocean circulation changes that occur during these transitions. A combination of an ocean global circulation model (OGCM) and a large–scale 3–D sediment transport model is used to model the global ocean thermohaline conveyor (THC) and distribution of the sedimentation rates for different time periods. Two different OGCM numerical mixing schemes are used to test the sensitivity of the sedimentation pattern to changes in model parameterizations of the thermohaline circulation, and especially the mixing technique. A sediment transport model is employed to identify glacial–to–interglacial changes of the deep–ocean currents. This model is suitable to identify the regions of the world ocean that are most responsive to the strong changes in glacial and interglacial circulation patterns and therefore are suitable for comparison of the computer simulations and geologic record. Two different eolian dust sources were prescribed at the sea surface: (1) A spatially homogeneous inorganic atmospheric dust source is used to depict sedimentation patterns that result only from the circulation changes. (2) A realistic present–day eolian dust pattern was specified in order to assess a more realistic sedimentation pattern. The results show that the modeled THC changes are traceable in the sediment accumulation patterns. These simulations indicate that the changes in sediment deposition rates are often associated with the changes in inter–basin water exchange, enabling verification of the simulated deep circulation using the geologic record.

INTRODUCTION

Decades of ocean sediment collection combined with major advances in ocean general circulation modeling provide a growing opportunity to address quantitatively a number of fascinating paleoceanographic problems. However, most of the existing sedimentation models are two–dimensional and are designed for small basins, targeting specific features such as alluvial or deltaic basin fill (cf. *Ericksen et al.* [1989]; *Tetzlaff and Harbaugh* [1989]; *Bitzer and Pflug* [1990]; *Paola et al.* [1992]; *Syvitski and Daughney* [1992]; *Cao and Lerche* [1994]; *Slingerland et al.* [1994]). In such models, sediment transport is gravity–driven, with the sediment load proportional to the basin slope, water discharge, and diffusion coefficient (e.g, *Granjeon and Joseph* [1999]). Usually, these models are not coupled with models that simulate the ocean general circulation. As such they are not capable of assessing the impact of global climate change on the ocean sediment

The Oceans and Rapid Climate Change: Past, Present, and Future
Geophysical Monograph 126

drifts on millennial and longer time scales. For these problems, a three–dimensional coupled ocean circulation–ocean sedimentation model is required. A coupled model is key to addressing the extent of the linkages between sedimentation and the deep–ocean, and whether modeled ocean paleocirculation can be unambiguously verified by observed changes in inorganic sedimentation rates and sediment drift dynamics. Our objective is to begin to assess whether it is possible to trace the changes in the total terrigenous sedimentation rates induced by millennium–scale changes of the ocean currents in a combined circulation–sedimentation model.

The following goals are pursued: (i) to simulate glacial–to–interglacial changes of the global ocean thermohaline conveyor; (ii) to test whether the deep–sea circulation signal is overwhelmed by changes in sediment input by simulating terrigenous (eolian) sedimentation rates for each conveyor regime with different sedimentation input rates and patterns; (iii) to test the method of using inorganic sediment as a tracer that can constrain past ocean circulation modeling. This study expands previous work by *Seidov and Haupt* [1997b] and *Seidov and Haupt* [1999] by addressing three additional questions: (1) Can we adequately specify an eolian sediment input at the sea surface in the sedimentation model? (2) Does the sediment transport by deep-ocean currents substantially modify the sedimentation pattern, or is the latter essentially determined by the input at the sea surface? (3) If the deep-ocean circulation can substantially influence the sedimentation rates, are there sufficient sediment data to verify the results of the simulations? Answering these questions is the main focus of this publication.

The global oceanic thermohaline circulation (THC), also known as the "salinity conveyor belt" [*Stommel*, 1958; *Broecker and Denton*, 1989; *Broecker*, 1991] is driven by deepwater production in the high-latitudes, especially by the production of North Atlantic Deep Water (NADW). The variability of deepwater formation in the North Atlantic has been addressed in a number of model studies during the last decade (e.g., *Maier-Reimer et al.* [1991]; *Manabe and Stouffer* [1988, 1995, 1997]; *Seidov and Haupt* [1999]; *Seidov and Maslin* [1999]). These studies show that changes in freshwater flux in the high–latitudinal North Atlantic (NA) can substantially modify the deep ocean circulation. Recent studies show that the NADW is not the only driver of the global conveyor belt (e.g., *Goodman* [1998]; *Stoessel et al.* [1998]; *Goosse and Fichefet* [1999]; *Scott et al.* [1999]; *Wang et al.* [1999]; *Seidov et al.* [2001a]). For example, a recent study by *Seidov et al.* [2001a] demonstrates that a relatively small disturbance in the freshwater flux in the present–day climate asymmetry, e.g. caused by melting of icebergs around Antarctica, could drastically change the THC. The study presented here is a companion to *Seidov et al.* [2001a] and *Seidov et al.* [2001b] (this volume) in that these contributions provide the circulation characteristics for the sediment transport simulations described here.

The effects of changes in glacial–to–interglacial interbasin water transport on sedimentation are evaluated by examining present–day and glacial ocean circulation experiments influenced by freshwater perturbations in the high latitudes of both hemispheres. The Late Quaternary and, more specifically, a scenario for the last glacial maximum (LGM) (22–18 ka BP) and for idealized subsequent meltwater events (MWE), are chosen as examples. The meltwater event scenarios in the Northern Hemisphere are designed to mimic real meltwater events caused by iceberg flotillas from either the Laurentide Ice Sheet (e.g., *Ruddiman and McIntyre* [1981]) or the Barents Ice Shelf (e.g., *Sarnthein et al.* [1994]). As these events substantially altered the deep–ocean circulation, we anticipate that they led to abrupt and noticeable changes in sedimentation patterns.

MODEL DESCRIPTIONS

A well–known ocean general circulation model (OGCM), the modular ocean model (MOM version 2.2, hereafter MOM) [*Bryan*, 1969; *Cox*, 1984; *Pacanowski et al.*, 1993; *MOM-2*, 1996], is utilized to compute the ocean circulation in order to drive sediment transport. The model domain is global for the ocean with a horizontal grid spacing of 6°x4° and 12 unequally spaced vertical layers. From top to bottom, the layer thicknesses are 100, 100, 100, 100, 100, 100, 200, 360, 584, 848, 1107, and 1301 m. The bathymetry with this resolution is derived from the *ETOPO5* [1986] data set and represents a smoothed version of the real World Ocean bottom topography (Figure 1). A rather coarse resolution is utilized, following other recent modeling efforts that target long–term climate change (e.g., *Toggweiler et al.* [1989]; *Manabe and Stouffer* [1995]; *Rahmstorf* [1995b]; *Seidov and Haupt* [1999]). A coarse resolution study is also justified by the limited amount of data for boundary conditions and for model verification [*Lessenger and Lerche*, 1999].

There are, however, many drawbacks to coarse resolution. For example, Iceland is represented by a seamount in the model bottom topography. Thus, velocity vectors, water mass transports, and non–zero sedimentation rates are artifacts at the exact position of this island. Even so, as we address scenario–type problems, we believe coarse resolution is sufficient in preliminary experiments. An important issue is whether the resolution of the models is appropriate to resolve 'sediment drifts', or if the results of

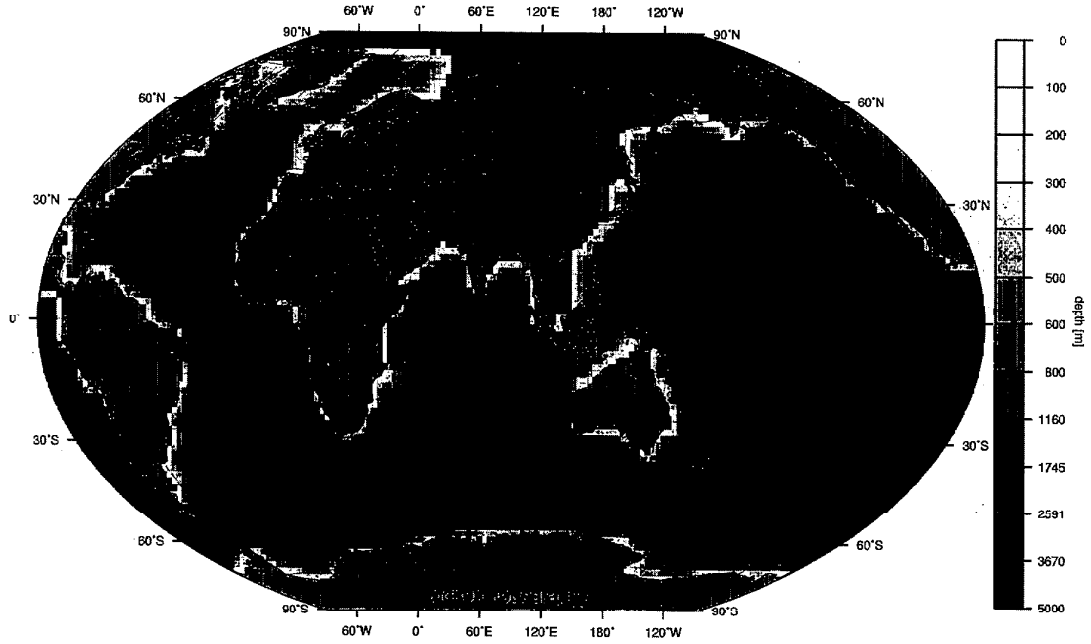

Figure 1. Model bathymetry with a horizontal grid spacing of 6°x4° and 12 unequally spaced vertical layers. The bathymetry is derived from the [*ETOPO5*, 1986] data set and represents a smoothed version of the real World Ocean bottom topography.

the sedimentation models merely indicate regions where they might occur. Clearly, such a coarse resolution does not allow identification of single known sediment drifts and waves, respectively, that are in close proximity. However, in previous studies *Haupt et al.* [1994], *Haupt* [1995], *Haupt et al.* [1995], *Stattegger et al.* [1997], *Haupt and Stattegger* [1999], *Haupt et al.* [1999], and *Seidov and Haupt* [1997b] showed with earlier versions of both OGCM and sediment transport models at much higher horizontal resolutions, 0.5°x0.5° and 2°x2° respectively, that the sediment transport model is capable of reproducing and distinguishing between 'small' drifts in the NA and around Iceland. Therefore, we mainly focus on the impact of glacial–to–interglacial changes in deep–ocean currents on the large–scale sedimentation patterns, especially in the areas of higher sediment accumulation, rather than on identification of single sediment drift bodies.

The off–line large–scale dynamic sediment transport model, SEDLOB, can be utilized to simulate: (1) sediment distribution patterns on the sea floor, especially accumulation and erosion of sediments integrated over time intervals long enough to represent the stratigraphic architecture; and (2) transport paths of water volumes and defined sediment particles from prescribed sources. SEDLOB consists of two components: a 3–D sediment transport model in the ocean interior and a 2–D sediment transport model in a near–bottom layer following smoothed bottom topography. The 3–D and 2–D sub-models are coupled by vertical exchange of suspended sediment. This exchange is crucial for redistribution of suspended sediment. Sediment suspended in the 2–D bottom layer (e.g., due to erosion) can re–enter the near-bottom 3–D currents. These currents are capable of transporting the suspended sediment to another deposition site (e.g., *Haupt et al.* [1994, 1995, 1999]; *Haupt and Stattegger* [1999]; see also discussion in *Beckmann* [1998]). This approach enables redistribution of sediment by the reduced bottom currents [*Sündermann and Klöcker*, 1983].

SEDLOB's 3–D component is used to simulate the lateral sediment transport and inorganic sediment material entry at the sea surface. This entry can include any kind of inorganic sediment including dust, ice–rafted debris and riverine sediment input. However, to simplify our task at this stage of the research, we include only eolian dust particles. The mass of sediment covering the seafloor depends only on the balance of sources and sinks, whereas the spatial variation of the sediment rate depends on the circulation pattern and particle grain size.

The sediment content of the 2–D bottom layer is updated at every time step by exchanging sediment between the main water body (near bottom water layer of the 3-D submodel) and the ocean floor (effectively the 2-D bottom

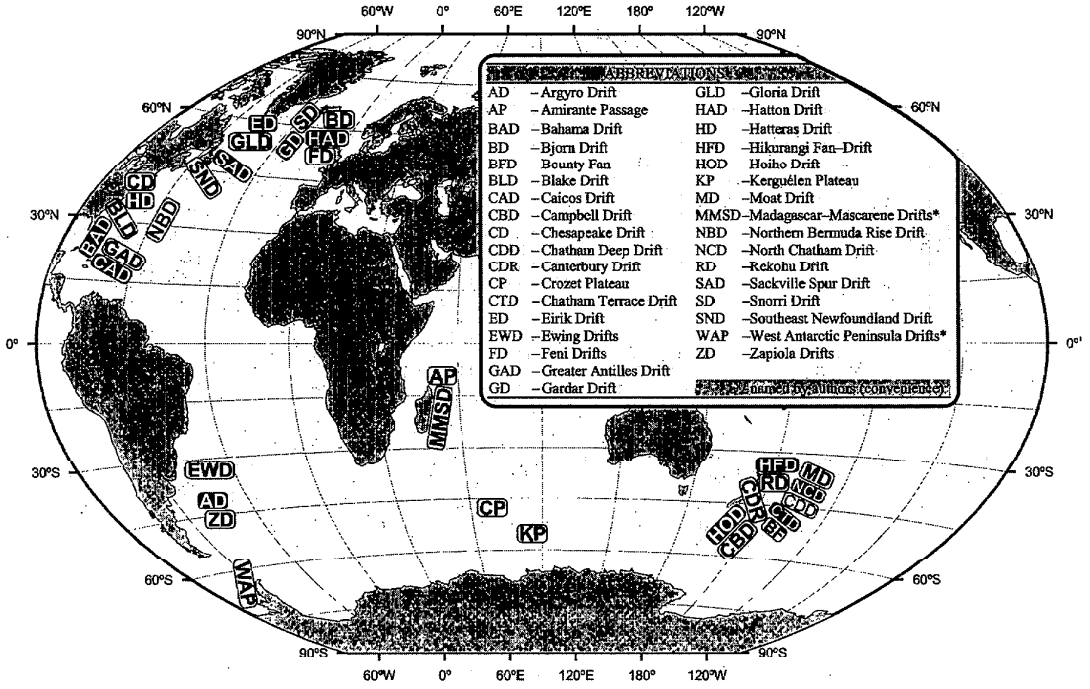

Figure 2. Locations of sediment drifts.

layer). The sediment in the bottom layer is transported by a corrected benthic flow, which is largely a projection of the OGCM velocity field onto the smoothed 1 cm thick bottom layer. Additionally, the near–bottom velocities are reduced as appropriate to take bottom friction into account [*Miller et al.*, 1977; *Sündermann and Klöcker*, 1983].

The equation for sediment concentration in the model is similar (except for the added settling term) to the OGCM equations for the 3-D advection–diffusion of heat and salt. This equation is solved numerically in the same way as in the OGCM, with horizontal and vertical mixing of sediment concentration and an added term describing sediment–settling rate.

Annual mean sea surface conditions are used in all experiments. The OGCM is run to steady state (see details in section 'Input Data and Setup of Numerical Experiments'). Thus, the OGCM provides velocity, temperature, salinity, and convection depths (in the locations where convection occurs due to hydrostatic instability) at steady state, which enter SEDLOB as external parameters. Internal variable parameters that are specified in SEDLOB are the sediment properties. Sediment source properties are characterized by their physical properties, sinking velocity of 0.05 cm s^{-1} = 43.2 m day^{-1} [*Shanks and Trent*, 1980], density (ρ_s = 2.6 g cm^{-3}) and porosity (γ = 0.75) of sediment, grain size and sedimentological grain diameter, and form factor of sediment particles (FF = 0.7) [*Zanke*, 1982]. SEDLOB can be coupled to any 3–D OGCM as long as adequate input fields (velocity, temperature, salinity, and convection depth) are provided (e.g., *Haupt et al.* [1994, 1995]; the most recent and detailed description of this model can be found in *Haupt and Stattegger* [1999] and *Haupt et al.* [1999]).

INPUT DATA AND SETUP OF NUMERICAL EXPERIMENTS

Near–bottom currents over the sediment layer consist of three major components: the water flows controlled by the sea surface conditions (i.e., by wind and heat, and freshwater fluxes across the sea surface), periodical tidal flows, and sporadic benthic flows caused by mesoscale eddies and other short–term processes (e.g., benthic storms). Our numerical experiments are based on mean currents (see model description). Consideration of other components of deep–ocean currents is beyond reasonable present–day computation capabilities. Moreover, the simulation of short–term components in a global ocean model is difficult because many events, such as turbidity currents and benthic storms, are often triggered by short-term atmospheric variability. *Flood and Shor* [1988] argue that if the effects of tidal and benthic storm flows are small, sediment drifts can be modeled using time–averaged deep–ocean currents with short–term variability filtered out. Furthermore, *Flood*

and Shor [1988] state that if benthic storms are common in a region, the impact of stationary currents cannot be traced in the sediment patterns because continuous, persistent near–bottom currents are needed to produce strong sediment drifts [*Flood and Shor*, 1988].

Three major glacial–to–interglacial modes of the conveyor are simulated. The output fields are used to model sedimentation patterns based on two different inorganic eolian atmospheric dust sources. The goal is to trace changes of THC in the transported, re–suspended, and re–deposited sediment over time intervals that are long enough to represent the stratigraphic changes in the sediment covering the sea floor. One group of experiments consists of the runs with highly idealized, spatially homogeneous eolian dust sources prescribed at the sea surface. These experiments have the goal of depicting only the circulation imprint in transporting eolian sediment. This homogeneous flux is equal 0.0864 mg m^{-2} day^{-1} [*Miller et al.*, 1977; *Honjo*, 1990]. Sediment deposition rates in these experiments are not real world rates. They are hypothetical sedimentation patterns calculated to explore the potential of the ocean circulation to transport the suspended material over the world ocean. In particular, these sedimentation rates illustrate differences between the near–bottom currents during the three major glacial–to–interglacial modes. Another set of experiments consists of runs with realistic present–day eolian dust patterns [*Rea*, 1994] with the objective of predicting a more realistic sedimentation pattern. Figure 3 shows the present–day eolian dust pattern (after *Rea* [1994]).

In the absence of the ocean currents (i.e., when sediment particles only settle downward and are not transported by the ocean flow), the pattern of sediment deposition rates repeats the pattern of the dust input at the surface. With currents, the spatial structure of deposition is entirely determined by the transportation, erosion, and re–deposition of sediment by the three-dimensional ocean currents. Although the model has the potential to include various biological organic sediment sources, such as dying plankton and fecal pellet production that can act as sediment sources, our first focus is only on the non–biogenic sediment because it behaves as a passive tracer and can be simulated without the complication of biochemical processes. For slow sinking particles like dust the issue is how they are transported from the ocean surface to the sea floor. For example, coccolith distribution at first appears to be puzzling because they project their distribution at the sea surface waters onto the sea floor without reflecting any features of the ocean currents. According to *Honjo* [1996] they take the fast track to the sea floor as fecal pellets or as aggregates instead of sinking as settling particles. Such biologically mediated aggregations of upper–ocean–

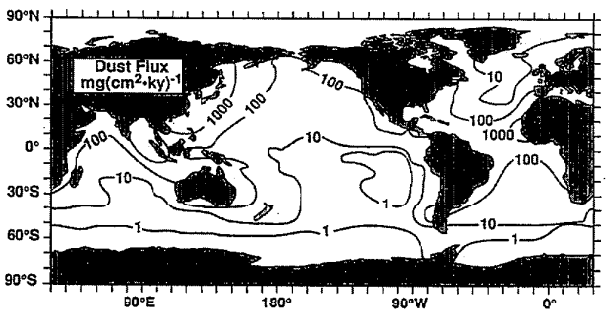

Figure 3. Estimate of the rate of deposition of mineral dust based on consideration of atmospheric transport (reproduced from [*Rea*, 1994], after [*Duce et al.*, 1991]).

generated particles settle much faster than individual fine particles. The bulk speed is up to 200 m d^{-1}. Here, we focus on non–biogenic and non–dissolvable particles that are slow settling and therefore can be transported by ocean currents.

Plate tectonic processes like continental displacement, subsidence, subduction, and sea–floor spreading, as well as sediment compaction are all neglected because they occur on much longer time scales than millennial–scale glacial cycles that we can simulate with reasonable computer resources. The glacial 100 m sea level lowering during the LGM [*Fairbanks*, 1989] including glaciation of shelf areas down to 200 m [*CLIMAP*, 1981; *Lehman*, 1991; *Mienert et al.*, 1992] is also disregarded because its effect on the global thermohaline circulation is minor.

Additionally, we investigate the effect of two different mixing schemes used in the OGCM on the sedimentation patterns as calculated with the sediment transport model SEDLOB (SEDimentation in Large Ocean Basins). Both models are briefly described below. Detailed descriptions of the SEDLOB model can be found in *Haupt et al.* [1999].

Previous numerical experiments using a combination of MOM and SEDLOB address three issues: (1) different numerical schemes used in MOM, (2) different climatic sea surface boundary conditions for different glacial–to–interglacial modes with variations in the sea surface salinity to test the impact of meltwater on the sedimentation pattern, and (3) different eolian sediment fluxes at the sea surface. Only those experiments that are shown in Table 1 (control runs for all three climatic modes) and Table 2 (sensitivity experiments) are discussed in the text. However, the conclusions are based on the large ensemble of runs that are represented in Tables 1 and 2. All OGCM runs are 2000 model years long, with a 5–fold acceleration in the deep layers (which means that the deep ocean is effectively run for 10,000 years). All have reached a complete steady state. For example, the global temperature and

Table 1. Control runs for three different climate scenarios, two different mixing schemes used in the OGCM, and two different eolian dust sources for SEDLOB. Note that experiments 1a and 1b as well as 2a and 2b have identical OGCM runs; they differ in the SEDLOB runs.

Exp.	time slice	OGCM mixing scheme	eolian dust source
#1a	PD	VAMS	H
#2a	PD	GMMS	H
#1b	PD	VAMS	PD–ADT
#2b	PD	GMMS	PD–ADT
#3	LGM	GMMS	PD–ADT
#4	MWE	GMMS	PD–ADT

OGCM – ocean general circulation model
GMMS – Gent–McWilliams [1990] isopycnal mixing scheme
VAMS – 'vertical adjustment' mixing scheme
LGM – last glacial maximum
MWE – meltwater event
PD – present–day
H – homogeneous inorganic eolian dust source instead of 'real' present–day distribution
PD–ADT – present–day atmospheric dust transport (reproduced from *Rea* [1994], after *Duce et al.* [1991]).

salinity changes for the last 100 model years are less than 10^{-4} °C and 10^{-5} psu, respectively. The tracer time step length is 86400s (1 day) and the time step length for velocity is 250 s. A more detailed view of the OGCM results is presented in another paper in this volume [*Seidov et al.*, 2001b].

The SEDLOB runs are 1000 years long to compute sedimentation rates for a particular climate state and circulation regime. Unlike the OGCM, it is not possible to run SEDLOB to a steady state condition. Forward time integration leads in every time step to continuous changes in the bottom slope, and therefore the critical velocities for initiating bed and suspension loads change as well, altering both bed and suspension load transports. These changes may influence maximum possible sediment concentrations and transport in the fluid because they are dependent. In fact, it may be viewed as an equivalent of changing sediment availability.

In the OGCM present–day control run, the upper layer of the ocean temperature and salinity are restored to the present–day sea surface climatology (PDC), that is to sea surface temperature (SST) and sea surface salinity (SSS). In the LGM and MWE control runs, the upper ocean temperature and salinity are restored to the sea surface climatology of the LGM and MWE (see above). Sea surface boundary conditions utilizing prescribed SST and SSS are outlined in detail in Table 1 in *Seidov and Haupt* [1999] (see also *Seidov et al.* [1996]; *Seidov and Haupt*, [1997a]). Additional discussion can be found in *Seidov et al.* [2001b] (this volume). Wind stress fields are from the Hamburg atmospheric circulation model, which was forced with present–day and glacial sea surface climatologies [*Lorenz et al.*, 1996]. For the LGM and MWE the same wind stress is used, although it has been shown that the alteration of wind stress in the Southern Ocean (SO) can by itself cause changes in the Atlantic deep–water circulation (e.g. *Toggweiler and Samuels* [1995]; *Rahmstorf and England* [1997]). We focus on the meltwater control, which provides a distinctive signature of glacial–to interglacial changes. Each of the OGCM control runs for a given climate state was performed twice: one set was done with the classical/conventional 'vertical adjustment' mixing scheme (VAMS) (convective adjustment) that mixes vertical thermohaline instabilities by averaging pairs of layers from top to bottom until all instabilities are removed [*MOM-2*, 1996]; the other set was done with the more sophisticated isopycnal mixing scheme developed by *Gent and McWilliams* [1990] and recently incorporated into MOM–2. Each of the runs with the OGCM found in Table 1 is accompanied by a corresponding SEDLOB run.

Exp.	NA	SO
#5	-3	–
#6	-3	+1
#7	–	-1
#8	–	+1

NA – North Atlantic
SO – Southern Ocean

Table 2. Present–day sensitivity experiments and their anomalies in psu. Salinity anomalies are added to the present–day annual mean sea surface salinity in the bands between 60°N and 80°N in NA, and a band between 50°S and the coast of the Antarctica (SO). The modified salinity was merged using a cosine filter to the unchanged field within two latitudinal grid points (8°). In the SO the anomalies are circumglobal. All OGCM runs were performed with the Gent–McWilliams [1990] isopycnal mixing scheme.

Another set of experiments combines sensitivity experiments that model freshwater surface impacts in either the Northern Hemisphere, Southern Hemisphere (SH), or in both hemispheres (Table 2; only the experiments using the Gent–McWilliams mixing scheme (GMMS) are presented). Furthermore, we use realistic present–day eolian dust patterns [*Rea*, 1994] (Figure 3) instead of the idealized homogenous source used in previous runs. Although the atmospheric dust load and its distribution are likely to have varied during glacial cycles [*Ram and Koenig*, 1997], we use the same present–day distribution for all three time slices (present–day, LGM, and MWE). The only justifica-

tion for such an approach is that we do not have reconstructed dust loads of the same quality for past times as we have for the present–day. In our first–order approach we only address the problem of whether ocean circulation changes can be seen in sedimentation patterns, provided that the dust load remains unchanged.

During the Quaternary, glaciation created an abundant source of eolian material. Deglaciation in regions of strong thermal contrasts and intensive winds created very large areas of unconsolidated glacial deposits [*Lisitzin*, 1996]. In contrast, terrigenous sediments are largely controlled by climatic zonality. As the distribution of aridity shifted with glaciation, the intensity of eolian deposits changed accordingly [*Lisitzin*, 1996; *Allen*, 1997]. Thus, eolian deposition rate is expected to increase during glaciation due to an increase in aridity. The atmosphere of the Northern Hemisphere has a higher concentration of eolian material than the SH today, and this asymmetry apparently also existed in the past. In the past, increases in wind speed had a strong impact on the dust transport and on oceanic sedimentation in the North Pacific (the largest in area), in the equatorial Atlantic and Indian Oceans, and in the regions adjacent to Australia [*Lisitzin*, 1996]. Although the aridity, wind speed and direction, and eolian sediment availability are known qualitatively for the last 20–30 thousand years, there is a great deal of uncertainty about the spatial distribution of eolian dust during LGM and MWE. Given this uncertainty the use of the same eolian sea surface sediment source for all three time slices is considered more useful for our study. However, the fact that these uncertainties could overwhelm the circulation differences in governing sediment patterns also introduces uncertainty in this study.

RESULTS AND DISCUSSION

The results of the experiments in Table 1 are discussed in the following sequence: (1) the results of changes in thermohaline circulation caused by different numerical mixing schemes used in the OGCM, and (2) the response of the thermohaline circulation to different sea surface boundary conditions for different geological time slices. In each case, the OGCM experiments are accompanied by calculation of sediment transport for two sea–surface sediment sources: (i) homogeneous eolian dust (constant everywhere), and (ii) a more realistic present–day eolian dust distribution over the sea surface [*Rea*, 1994].

The Effect of the Mixing Scheme on the Thermohaline Circulation

The key–element of the present–day meridional circulation is the southward North Atlantic Deepwater (NADW)

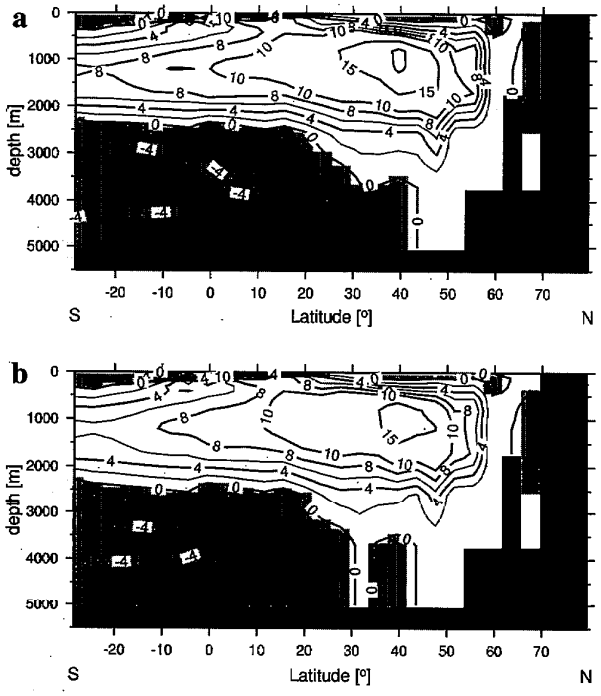

Figure 4. Meridional overturning in the Atlantic Ocean for the present–day experiments (in Sv; 1 Sv = 10^6 m^3s^{-1}): (a) Exp. 1a and (b) Exp. 1b. The positive values depict clockwise motion while negative values (shaded) depict counterclockwise motion. The Atlantic overturning is valid only within this ocean's geographical boundary (with meridional walls at both sides; therefore the area south of 30°S is not shown).

outflow from convection sites in the northern North Atlantic (NNA). Figure 4 shows the Atlantic meridional overturning stream function (in Sverdrups (Sv); 1 Sv = 10^6 m^3s^{-1}), a representation of the zonally averaged and depth integrated meridional ocean circulation, for the VAMS (Figure 4a) and the GMMS (Figure 4b). Except for the different mixing schemes, all parameters were kept identical in both experiments. Although the overturning looks reasonable in both of the runs, there are important differences that reflect differences in the numerical schemes. The NADW penetrates to the same depths in both runs, but the production rate is 20 Sv in the VAMS run and only 15 Sv in GMMS experiment. Both are within the estimated NADW production rates [*Schmitz*, 1995]. AABW production rates are 6 Sv (GMMS) and 8 Sv (VAMS), which is again in good agreement with climatic averages [*Schmitz*, 1995].

Another way to illustrate the magnitude of the three–dimensional horizontal circulation is to show the water volume transport across vertical diagonal sections of the model's grid cells in Sv. For this purpose we multiplied the

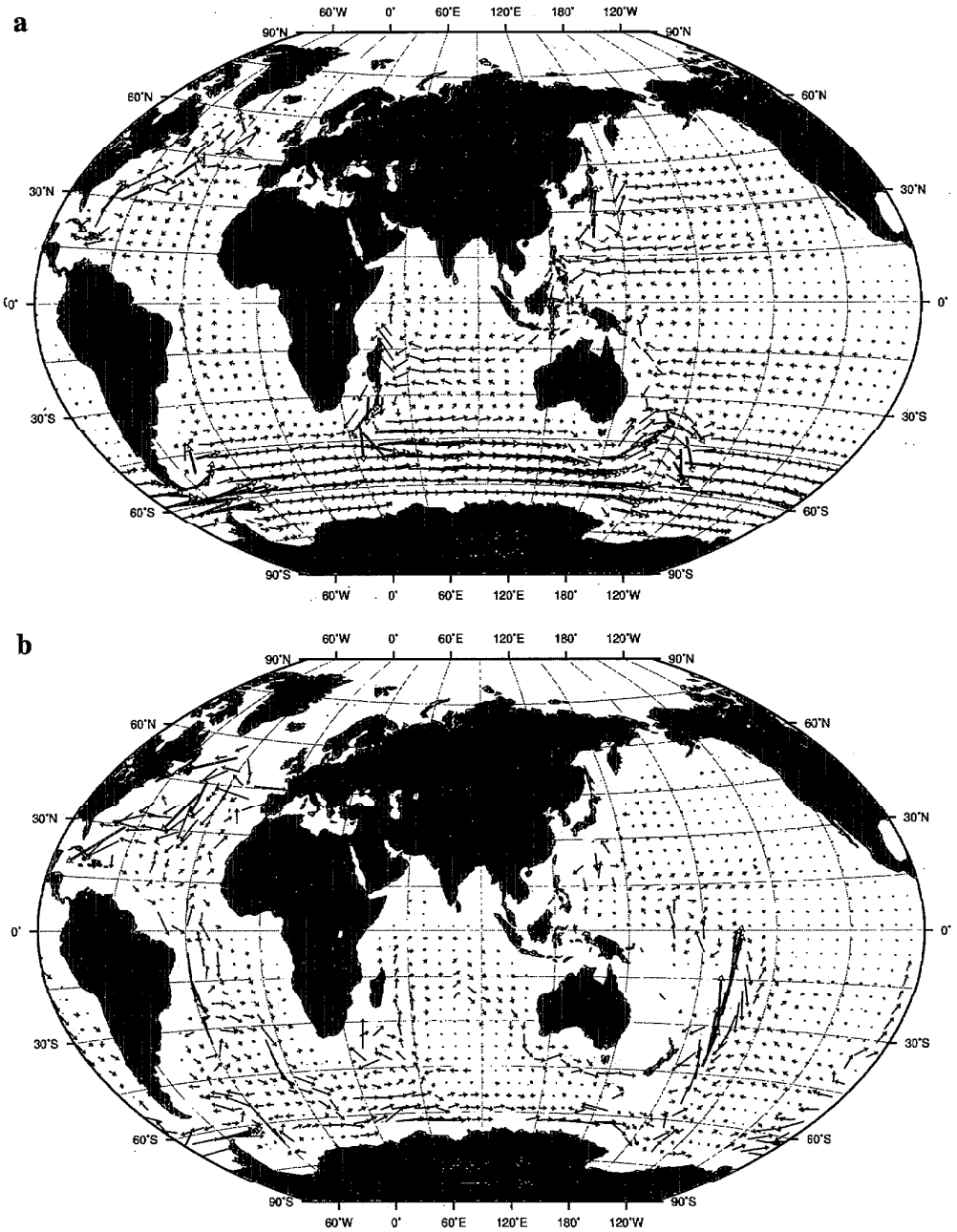

Figure 5. Total water mass transport from Exp. 1a across vertical sections of the grid cells in Sv (1 Sv = 10^6 m^3s^{-1}): a) upper (above 1.5 km) ocean transport; b) deep (below 1.5 km) ocean transport. Note different scales of vectors for upper and deep ocean.

horizontal velocity components by the area of the side surfaces of the grid cells, and summed vertically from the sea surface to 1.5 km (upper ocean) and from 1.5 km to the bottom (deep ocean). Figure 5 depicts the present–day conveyor mode (Exp.1a) with a strong deep ocean flow of NADW that penetrates the Antarctic Circumpolar Current (ACC). Then, carried by the ACC in the deep ocean, NADW spreads into the Indian and Pacific oceans.

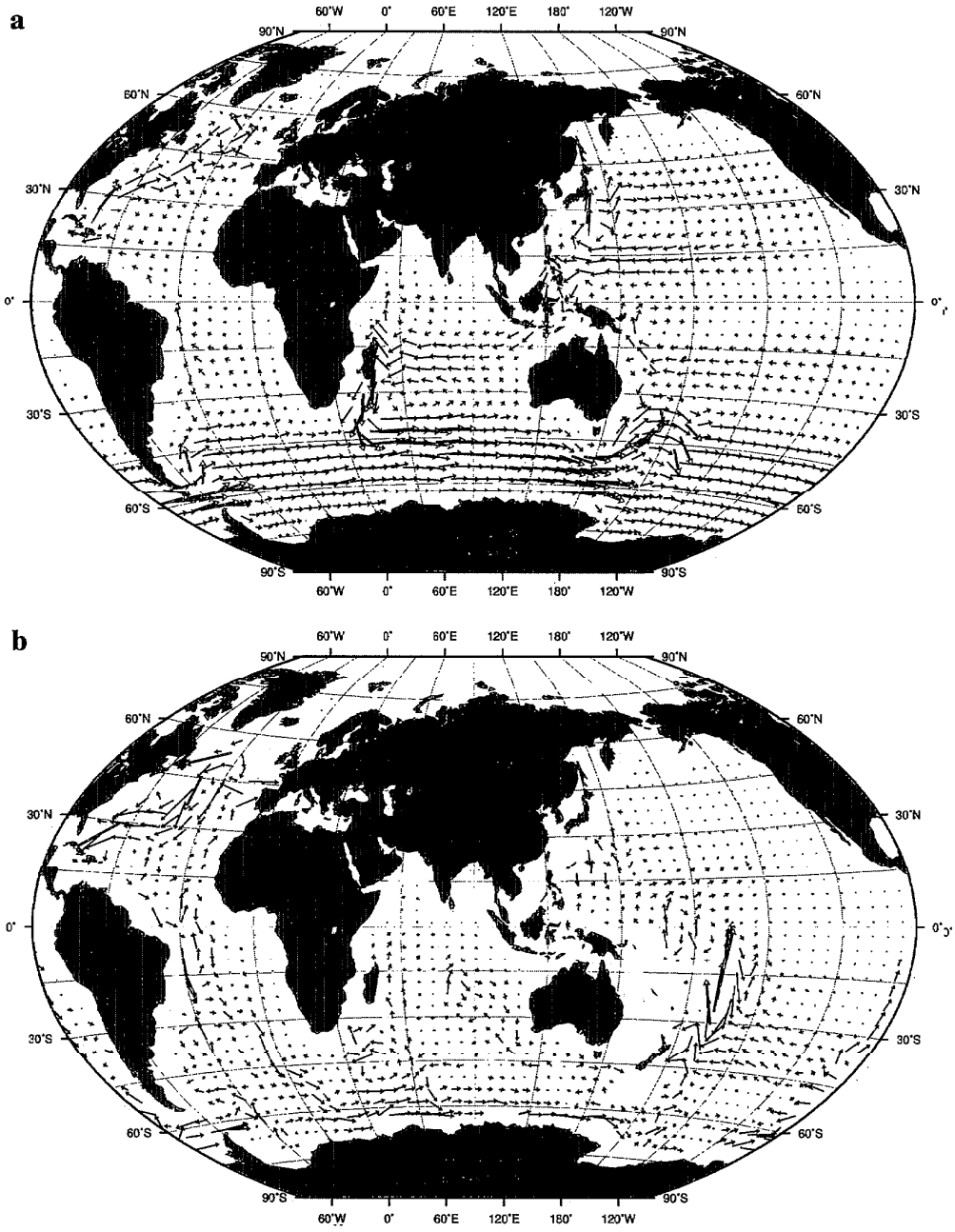

Figure 6. As Figure 5 for Exp. 2a.

Horizontal water mass transport in the upper and deep ocean layers is shown for Exp. 2a in Figure 6. The three–dimensional currents are far more complex than the vertically integrated flows shown in Figures 5 and 6. For example, the deep inflow of the Antarctic Bottom Water (AABW) into the central and NA is masked in these figures. However, integrated volume transports do give a good schematic view of the global thermohaline conveyor.

Deep–ocean currents show stronger sensitivity to millennial–scale climate changes than the surface currents (e.g. *Seidov and Haupt* [1997a]). Moreover in case of re–suspension, deep–ocean flow can effectively influence the

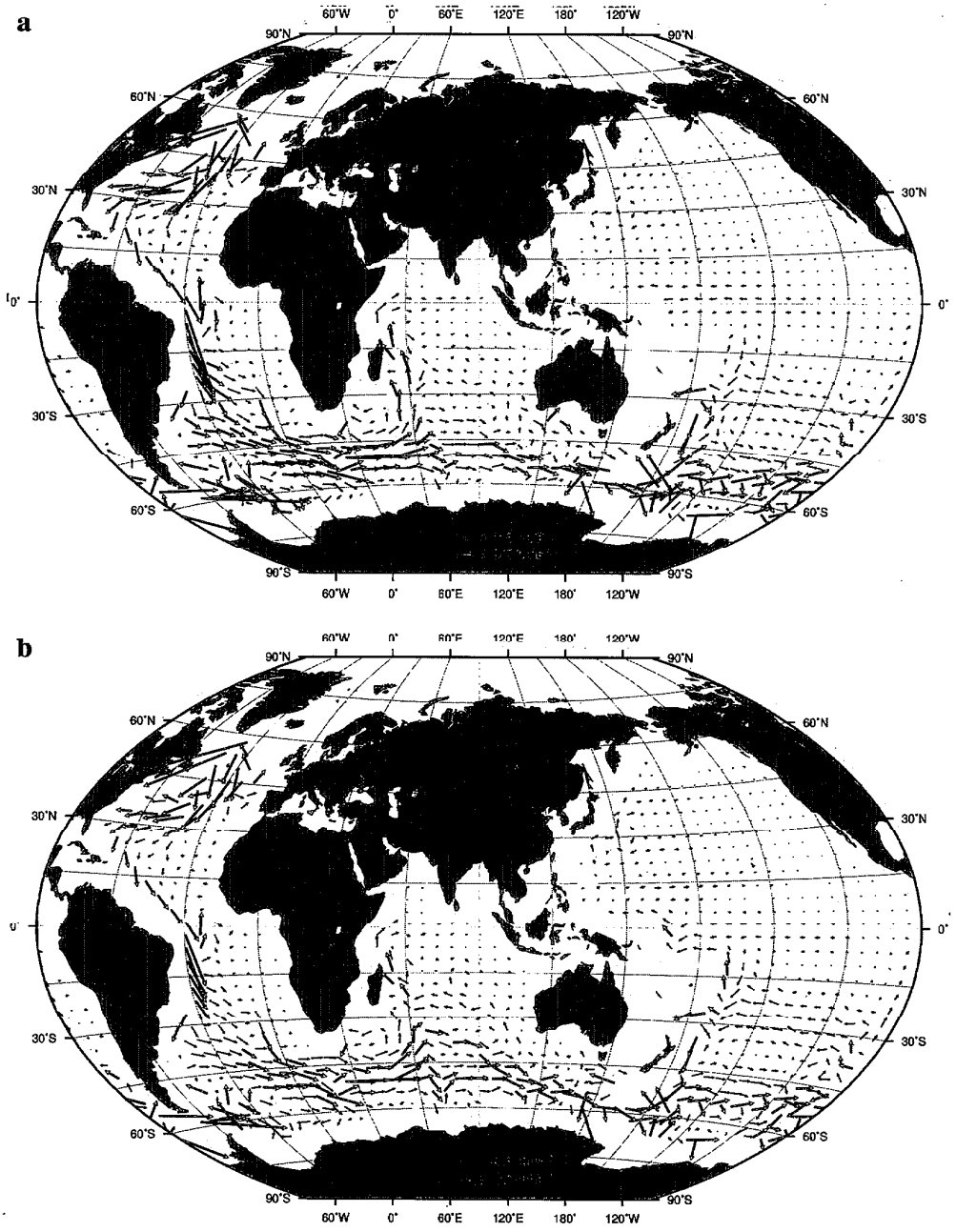

Figure 7. Velocity vectors (in cm s^{-1}) at 2.5 km: a) Exp. 1a; Exp. 2a.

sediment drifts. Figure 7 depicts the present–day circulation at 2.5 km depth for the VAMS (Figure 7a) and GMMS (Figure 7b). It appears that deep ocean currents are not very different in the VAMS and GMMS runs. Figures 5–7 show weaker western boundary currents and a weaker Antarctic Circumpolar Current in the GMMS experiment. The water mass transport in Sv across selected meridional and zonal vertical sections for different depths in different oceans is depicted in Figure 8a (Exp. 1a) and 8b (Exp. 2a) illustrating water volume exchanges between different parts of the world ocean. In some cases, volume transports in three, rather than in two layers are shown to differentiate

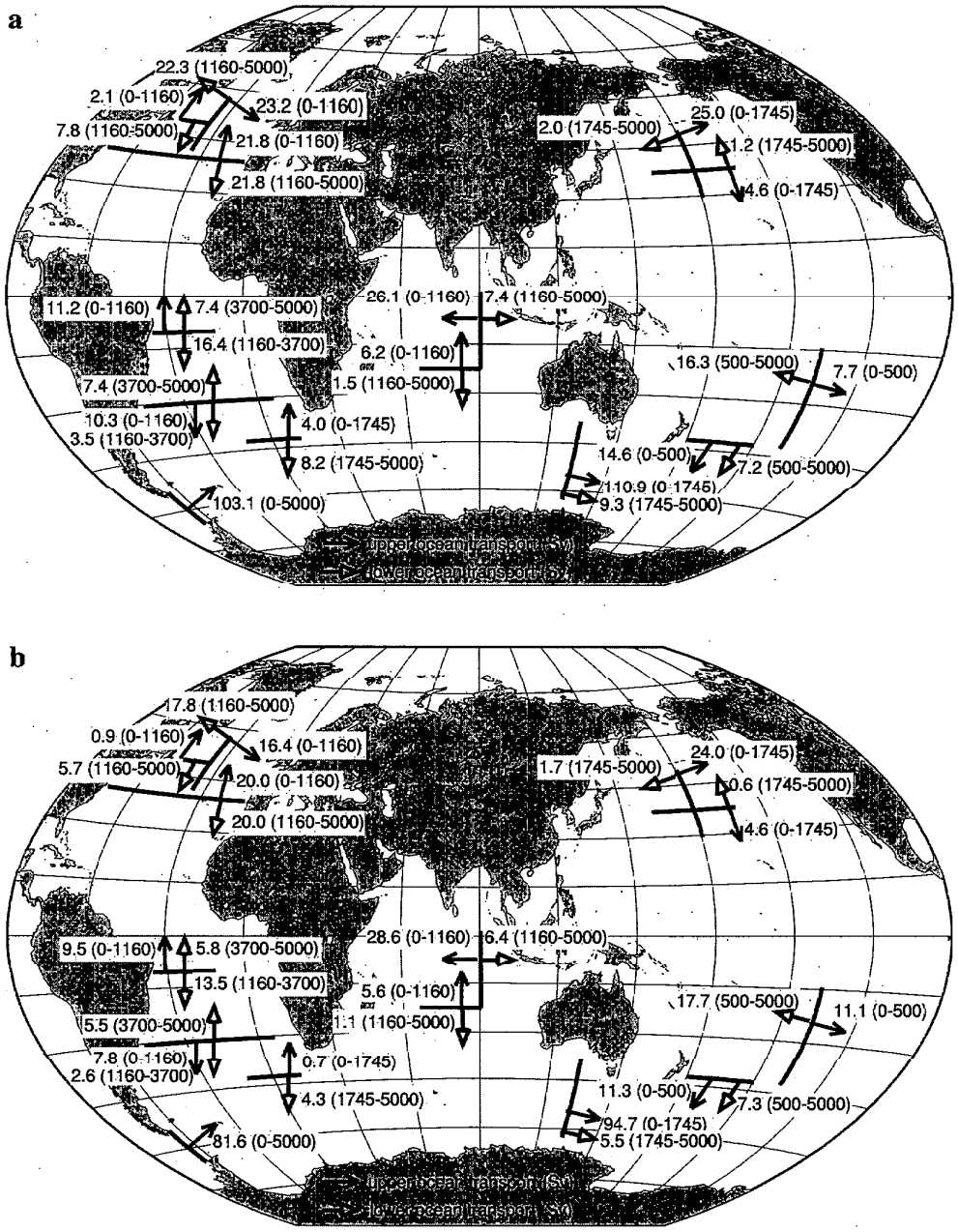

Figure 8. The water mass transport in Sv (1 Sverdrup (Sv) = 10^6 m^3s^{-1}) across chosen meridional and zonal vertical sections for different depths in different oceans: a) Exp. 1a and b) Exp. 2a. Primarily, the transports in the upper and deep ocean are shown; in cases when upper and intermediate water movement essentially differs, the transports in three layers are shown to differentiate between the upper, intermediate–to–deep, and deep–to abyssal flows.

between the flows in the upper, intermediate–to–deep, and deep–to–abyssal flows.

As *Seidov and Haupt* [1999] used VAMS, the results of Exp. 1a shown in Figure 4a, 5, 6a, and 7a match their results better than those obtained with GMMS. However, there are substantial differences between the two numerical schemes used in the OGCM. Because GMMS is accepted as the most advanced mixing scheme [*Pacanowski*, 1996],

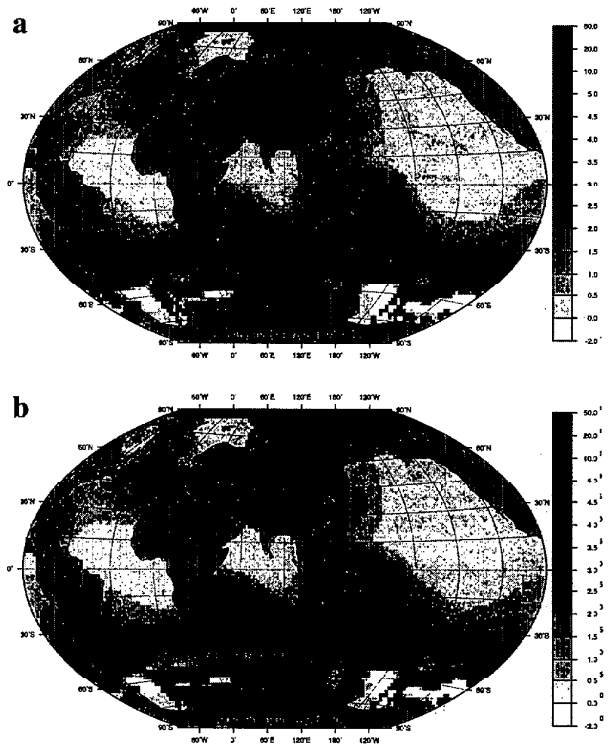

Figure 9. Sedimentation rates from Exp. 1a and (b) Exp. 2a. The color bar gives the sedimentation rates in cm/1000 years. The sedimentation rates shown are not realistic because of an idealized character of the sea surface eolian sediment source.

all of the sections that follow which discuss sensitivity experiments targeting glacial–interglacial changes are based on GMMS. The new results, shown in the next sections, can be considered as an improvement over *Seidov and Haupt* [1999].

The Effect of the Mixing Scheme on the Sedimentation Pattern

The sedimentation patterns have been reconstructed for the global ocean using spatially homogeneous eolian dust supply at the sea surface. Plate 2a shows the results of Exp. 1a whereas Plate 2b shows the computed sediment distribution of Exp. 2a. Using the homogeneous sediment source, the sedimentation rates are not realistic, but they do act as a passive tracer of the circulation. Even though observed sediment distributions cannot be used for a direct model–observation comparison, there are a number of known sediment drifts that reflect development times of tens to hundreds of thousands of years. These drifts, invariably formed in fine–grained sediments, reflect a long–term response to environmental conditions rather than a short–term response to discrete events [*Flood and Shor*, 1988]. Their presence has often been used as an indicator of the environment associated with sediment deposited from steady, sediment–laden flows. This correlation may help to trace the role of deep–ocean currents in creating and maintaining large–scale sediment drifts.

The simulated sedimentation patterns (not the total amount of sediment) shown in Figure 9 are slightly different from those in *Seidov and Haupt* [1999] (compare with Plate 1a in *Seidov and Haupt* [1999]; note the different scale). There are two possible reasons for the differences: (a) *Seidov and Haupt* [1999] used an older version of MOM (version 1), and (b) the tuning of present–day sea surface salinity required to produce "observed" NADW rates differed slightly (see *Seidov et al.* [1996]). However, the two simulations are generally in a good agreement. For example, higher sedimentation rates are associated with the present–day conveyor mode south of Iceland, in the Caribbean Sea, and in most other key regions, including the southern part of the Argentine Basin, the Cape and Agulhas Basin, and areas east of Australia and New Zealand (Exp. 1a and 2a). These locations of high sediment deposition rates are in agreement with the present–day concept of trapping of inorganic eolian sediment in these areas [*McCave and Tucholke*, 1986; *Bohrmann et al.*, 1990]. Although the sedimentation rates in the western NA are not as high as indicated by the geological record, our modeled results show increased sedimentation in the western NA along the deep western southward flowing boundary current. *McCave and Tucholke* [1986] argue that high sedimentation rates are in the areas of maximum kinetic energy in the western boundary currents.

In the South Atlantic, our model predicts high sedimentation rates in the southern part of the Argentine Basin in the area of the Falkland Escarpment (~50°S, ~55–40°W). This high sediment accumulation can be linked to the Zapiola Drift produced by the Falkland Current [*Flood and Shor*, 1988]. In the Indian Ocean, SEDLOB gives high sedimentation rates in the Cape and Agulhas Basins. This is in agreement with observations (e.g. *Hollister and McCave* [1984]; *Faugeres et al.* [1993]). The map of suspended material load by *Hollister and McCave* [1984] corresponds to the high kinetic energy of surface currents and the spread of cold deep–ocean water flowing northward. SEDLOB also gives high sedimentation rates southeast of New Zealand. These drifts may be under control of the East Australian Current.

Model sediment thicknesses maxima (higher values than in the surrounding basins) match the geologic record in the Yellow Sea and East China Sea [*Nittrouer and Wright*, 1994]. In the real world, the sediment accumulation is, in

general, much higher than in the model. If added, the riverine inputs, e.g., from the Huanghe (Yellow River), running into the Gulf of Bohai could be substantial regional source [*Nittrouer and Wright*, 1994]. However, for large–scale open–ocean patterns this source is not essential to tracing the deep ocean currents (see above).

The model's low Pacific sedimentation rate in the central North Pacific is also consistent with measurements [*Rea et al.*, 1985] (see also e.g., *Lisitzin* [1996]). Sedimentation rates derived from their data range from a minimum of 0.02 cm/ka (30°N) to a maximum of about 1.4 cm/ka (40°N).

The model sediment deposition rates around Antarctica are too high. This may be caused by overestimated sediment supply at the sea surface in this region, as represented by our idealized homogeneous boundary conditions. *Rea* [1994] indicates that Antarctica does not substantially contribute eolian dust to the world ocean (see also e.g., *Lisitzin* [1996]) (compare Figure 3). There are mainly two reasons for this: (1) the wind around Antarctica blows predominantly parallel to or even towards the shoreline, (2) Antarctica is covered by ice and delivers very little dust, and (3) part of the SO is covered by sea ice shielding the ocean from eolian source.

An overall comparison of the two experiments, Exp. 1a and 2a, shows that the sedimentation rates in Exp. 2a, especially near the western boundary currents, are slightly smaller than in Exp. 1a. As we use the same initial sea surface boundary conditions in both OGCM runs, this discrepancy represents the difference between the GMMS and the VAMS. However, except for smaller–scale details, these two numerical mixing schemes do not produce significantly different large–scale deep–sea sediment distributions. The experiments which follow are based only on the results obtained using MOM 2 with the more advanced GMMS mixing scheme.

The Effect of Climate Variability on Deep–Sea Sedimentation

In this section, we focus on the linkage between changes in the sedimentation rates in key areas and changes in the water transports during glacial–to–interglacial cycles. Plate 1 shows sedimentation rates in Exp. 2b, Exp. 3, and Exp. 4. In contrast with the idealized simulations described in the previous section, a realistic present–day surface dust distribution from *Rea* [1994] (Figure 3) is employed. Thus, we now focus on changes in deep–sea sediment deposition caused by changes in deep–sea circulation and inter–basin water exchange as a result of climatic variability that can be more directly compared to present–day observations.

Present–day sediment distribution. The simulated present–day sediment distribution is shown in Plate 1a. The sedimentation pattern in Plate 1a differs from that in Figure 9b. There are many regions where the differences are substantial. For example, the sediment accumulation is higher in the Sea of Japan, the Coral Sea northeast of Australia, the North American Basin, in the Caribbean Sea, under the Gulf Stream System [*Hollister and McCave*, 1984], the southern part of the Argentine Basin (approximately 50°S), the Falkland Escarpment, and in particular, in the Zapiola Drift. The high sedimentation rates in the Zapiola Drift are consistent with observations (e.g., *Flood and Shor* [1988]). Also, we find good agreement between modeled and observed (e.g., *Johnson and Damuth* [1979]) patterns east and northeast of Madagascar and in the Mozambique Channel. *Johnson and Damuth* [1979] state that these drifts were produced by the deep western boundary current in the Indian Ocean (IDWBC), which flows northward along the western margins of the Madagascar Basin through the Mascarene Basin and then through the Amirante Passage into the Somali Basin [*Kolla et al.*, 1980]. The thickness of the drift deposits in the passage suggests that the IDWBC has been active for several to tens of million years. Therefore, the model should predict high sedimentation rates in the IDWBC region for all three time slices in these simulations (compare Plate 1b, c) [*Johnson and Damuth*, 1979; *Kolla et al.*, 1980].

In the eastern part of the Argentine Basin the model predicts a high accumulation area seaward from the edge of the continental shelf. There are other separate sediment drifts in this area, for example the Argyro Drifts and the Ewing Drifts [*Faugeres et al.*, 1993]. Although our coarse horizontal grid resolution does not distinguish between different drift bodies, it does predict that major sediment drifts should be found within the Argentine Basin. This result is in good agreement with the modeled and observed undirected flow pattern in this basin, a basin where major sediment drifts are found mostly out outside the area of benthic storms [*Flood and Shor*, 1988]. *Flood and Shor* [1988] mention that the resolution of their 3.5 kHz profiles is not sufficient to determine Holocene sedimentation rates because the post–glacial sediment is not thick enough. Therefore, it is difficult to compare the modeled sedimentation rates with observations.

Smaller areas of accumulation that also match observations (e.g., *Rebesco et al.* [1994]) were found along the continental rise west of the Antarctic Peninsula between 63 and 69°S. In this region, a group of eight mud waves has been detected [*Rebesco et al.*, 1994]. *Rebesco et al.* [1994] identified the northern four mounds as sediment drifts in the area where the currents weaken and turn northeastward. Again, in coarse resolution simulations one cannot resolve small drift bodies, yet the pattern of large–scale sedimentation in the area is considered an acceptable match.

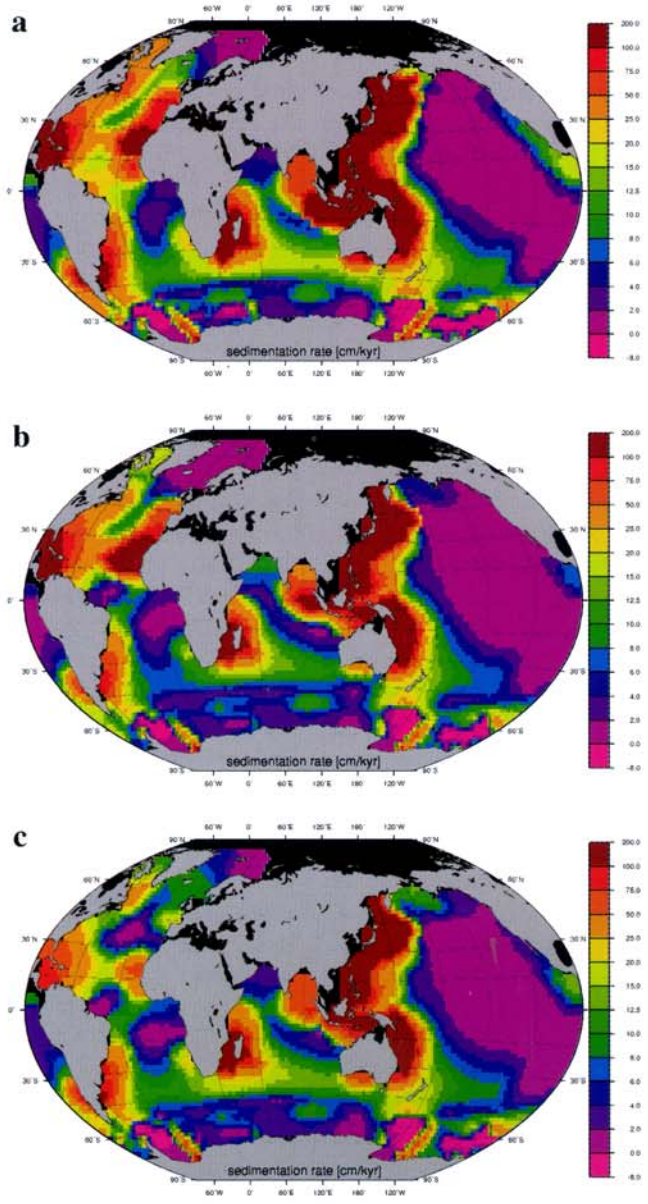

Plate 1. Sedimentation rates from Exp. 2b (a), Exp. 3 (b), and Exp. 4 (c). The color bar gives the sedimentation rates in cm/1000 years. All three climate scenarios were forced with the present–day sea surface eolian sediment distribution [*Rea*, 1994]. The goal is to link the changes of sediment drifts to changes of the ocean circulation patterns and inter–basin water exchange (see text).

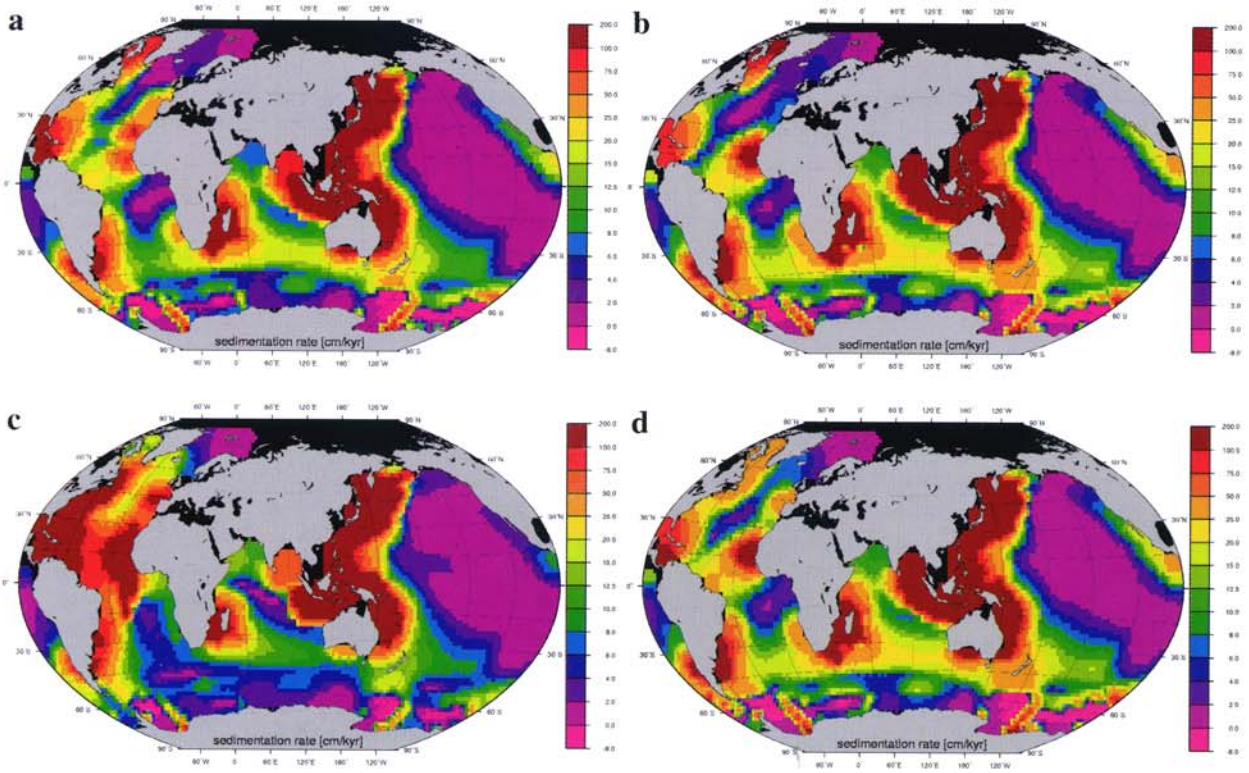

Plate 2. Sedimentation rates from Exp. 5 (a), Exp. 6 (b) Exp. 7 (a), and Exp. 8 (d). The color bar gives the scale of the thickness (in cm) of sediment accumulated during 1000 years, or sedimentation rates in cm/1000 years. All three climate scenarios were forced with the present–day sea surface eolian sediment distribution [*Rea*, 1994]. The goal is to link the changes of sediment drifts to changes of the ocean circulation patterns and inter–basin water exchange (see text).

Despite substantial differences in surface dust sources – between the idealized homogeneous, and observed present–day fluxes –, many high accumulation areas (e.g., the Hikurangi Fan–drift, Moat Drift, North Chathman Drift, Chathman Deep Drift, Chathman Terrace Drift, Canterbury Drift, Bounty Fan, Hoiho Drift, and Campbell Drift) east, southeast, and south of New Zealand [*Carter and Mitchell*, 1987] have similar shape (compare results from Exp. 1b and 2a) albeit higher rates. This result reflects the fact that the deep–ocean currents are not very different. For example, forty percent of the Earth's cold deep water enters the Southwest Pacific as the world largest deep western boundary current (SWP–DWBC), the so–called western intensification, flowing northward at bathyal to abyssal depths, east of New Zealand. South of 50°S, the SWP–DWBC is intimately linked with the ACC [*Carter et al.*, 1996]. *Carter et al.* [1996] argue that the eastern New Zealand oceanic sedimentary system is on a margin where sediment supply was steady for at least 10 My (compare sedimentation pattern in this region for LGM (Plate 1b) and MWE (Plate 1c)).

There are several other areas where sediment accumulation can be linked to highly energetic deep western boundary currents (DWBC) [*Hollister and McCave*, 1984]. For example, the high sedimentation area in the Tasman Sea is beneath the East Australian Current and, over large areas, is beneath the Antarctic Circumpolar Current – southeast of the Crozet Plateau near the Kerguelen Plateau.

Exp. 2b shows a large sediment buildup in the subtropical North Atlantic in comparison to Exp. 2a, since eolian material is more abundant in the air of the Atlantic Ocean of the northern hemisphere than anywhere else [*Lisitzin*, 1996] (Figure 3). This may be caused by increased concentration of eolian dust off the Sahara [*Lisitzin*, 1996; *Allen*, 1997]. Satellite images show that during much of the year several hundred million tons of African dust is transported primarily toward the Caribbean [*Prospero*, 1996; *Prospero et al.*, 1996; *Shinn et al.*, 2000]. With seasonally shifting winds and ocean currents, the dust is also deposited in the Gulf of Mexico and equatorial regions of South America [*Shinn et al.*, 2000]. There are other large regions influenced by the higher concentration of dust in the atmosphere of the Northern Hemisphere in comparison with the Southern Hemisphere. For example, the equatorial Indian Ocean and the western part of the North Pacific receive large amounts of dust from Asia [*Lisitzin*, 1996; *Allen*, 1997]. In the Southern Hemisphere the continental shelf and regions of the deep ocean adjacent to Australia receive their eolian sediment as the dust coming from Australian deserts [*Lisitzin*, 1996; *Allen*, 1997]. Our model results reflect these features in the runs with the realistic dust supply at the surface. Yet, ocean circulation imposes significant impact on the fate of eolian sediment.

For instance, before applying the realistic eolian dust source to SEDLOB, we expected high accumulation everywhere in the deep sea where the dust concentration is high at the surface. Surprisingly, this is not always true in our simulations. Although the atmospheric dust concentration is high in the Arabian Sea, the model predicts relatively low sediment–settling rates for this region when compared to the adjoining basins due to the role of currents.

A lack of correlation between the surface supply and bottom accumulation is also found in the Bay of Bengal and several other regions. In the Arabian Sea, for example, simulated sedimentation rates are, by an order of magnitude higher due to a higher eolian dust supply. However, the model sedimentation rates in the northern part of the Indian Ocean are much lower than observed. The reason for this discrepancy is the lack of strong riverine sediment input in our simulations (riverine sediment discharge is responsible at least for approximately 90% of sediment deposition [*Lisitzin*, 1996]).

Glacial sediment distribution. Both paleoreconstructions and ocean modeling indicate that the global ocean thermohaline conveyor worked differently in the past than it works now (e.g., *Boyle and Keigwin* [1987]; *Broecker* [1991]; *Crowley and Kim* [1992]; *Maier-Reimer et al.* [1993]; *Weaver et al.* [1993]; *Fichefet et al.* [1994]; *Rahmstorf* [1994, 1995a]; *Manabe and Stouffer* [1997]; *Ganopolski et al.* [1998]; *Seidov and Haupt* [1999]). Our simulations are in good agreement with these publications. NADW production was much weaker during the LGM than today. Figure 10 depicts the LGM conveyor mode (Exp. 3) with its weakened flow of NADW penetrating the ACC (Figure 11a). Figure 12a shows glacial meridional overturning in the Atlantic Ocean with a maximum of approximately 8 Sv, about 30% less than today. Northward heat transport in the Atlantic is weaker because of the reduced meridional overturning (Figure 13). The present–day North Atlantic current brings about 6 Sv into the Nordic Seas (Exp. 2b). During the LGM there is almost no inflow (0.2 Sv). Here we show that the differences in the circulation regimes are traceable in the pattern of sedimentation (see also *Seidov and Haupt* [1999]). Plate 1b displays sediment patterns in a LGM simulation (Table 1, Exp. 3). Reduction of the North Atlantic current carrying suspended sediment northward leads to lower sedimentation rates around Iceland (Plate 1b). Along with this reduction, a concurrent predicted increase in sedimentation rates in the eastern NA is strongly supported by reconstructions indicating stronger glacial sedimentation along the eastern

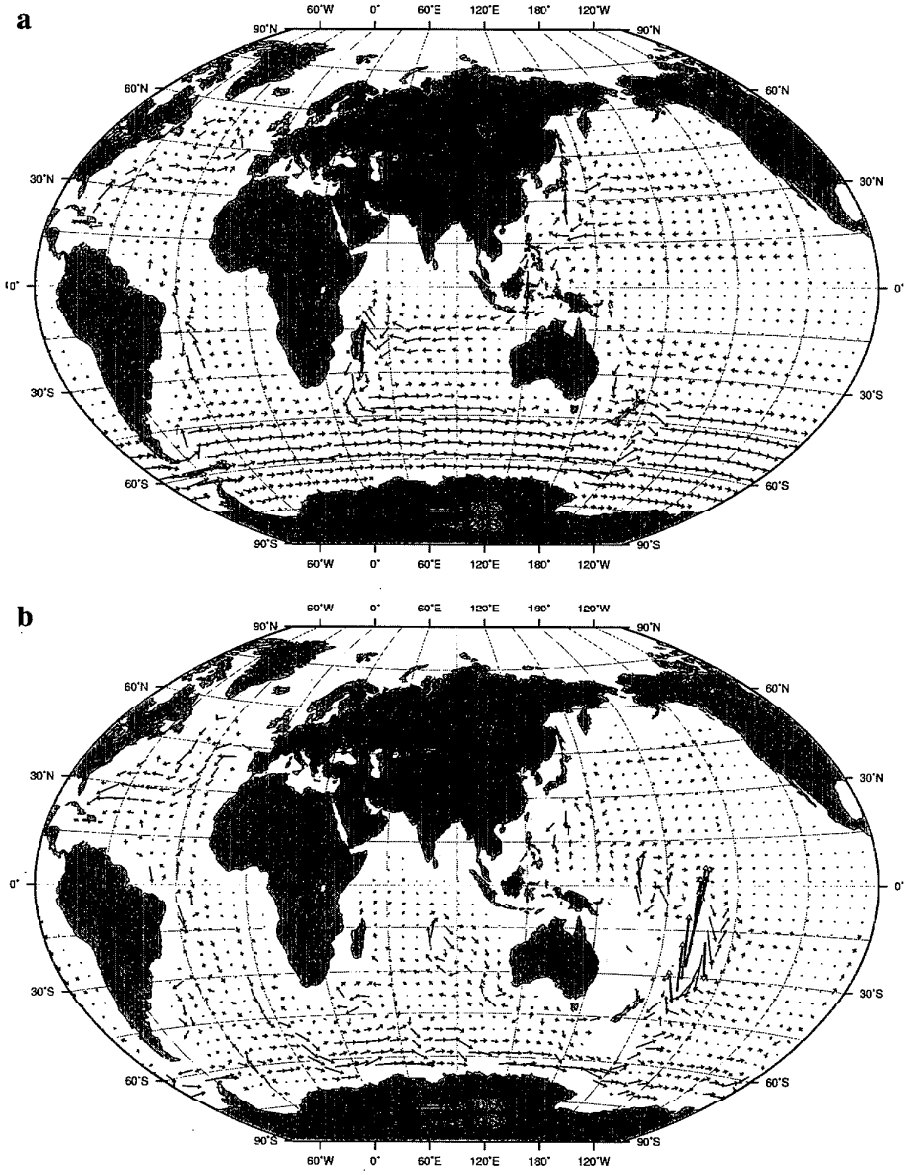

Figure 10. Total water mass transport for the LGM (Exp. 3) across vertical sections of the grid cells in Sv (1 Sverdrup (Sv) = 10^6 m^3s^{-1}): a) upper (above 1.5 km) ocean transport; b) deep (below 1.5 km) ocean transport. Note different scales of vectors for upper and deep ocean.

flank of the Mid–Atlantic Ridge (e.g., *Dowling and McCave* [1993]; *Robinson and McCave* [1994]). High glacial sedimentation rates are found west of the North African coast. Dust from the Sahara and Sahel is found in sediment thousands of kilometers away, as far away as in the Caribbean Basin [*Allen*, 1997]. As we use present–day rather than genuine glacial dust patterns (Saharan dust input in the Atlantic is thought to have been twice as high as today [*Kolla et al.*, 1980], during glacial times), the model tends to underestimate sediment accumulation in these areas.

In the LGM experiment, the sedimentation rates in the Nordic Seas around Iceland are also lower than observed. Although the winds during glacial times were not generally stronger [*Rea*, 1994], continental dust concentrations in Greenland ice older than 10750 years indicate an increased

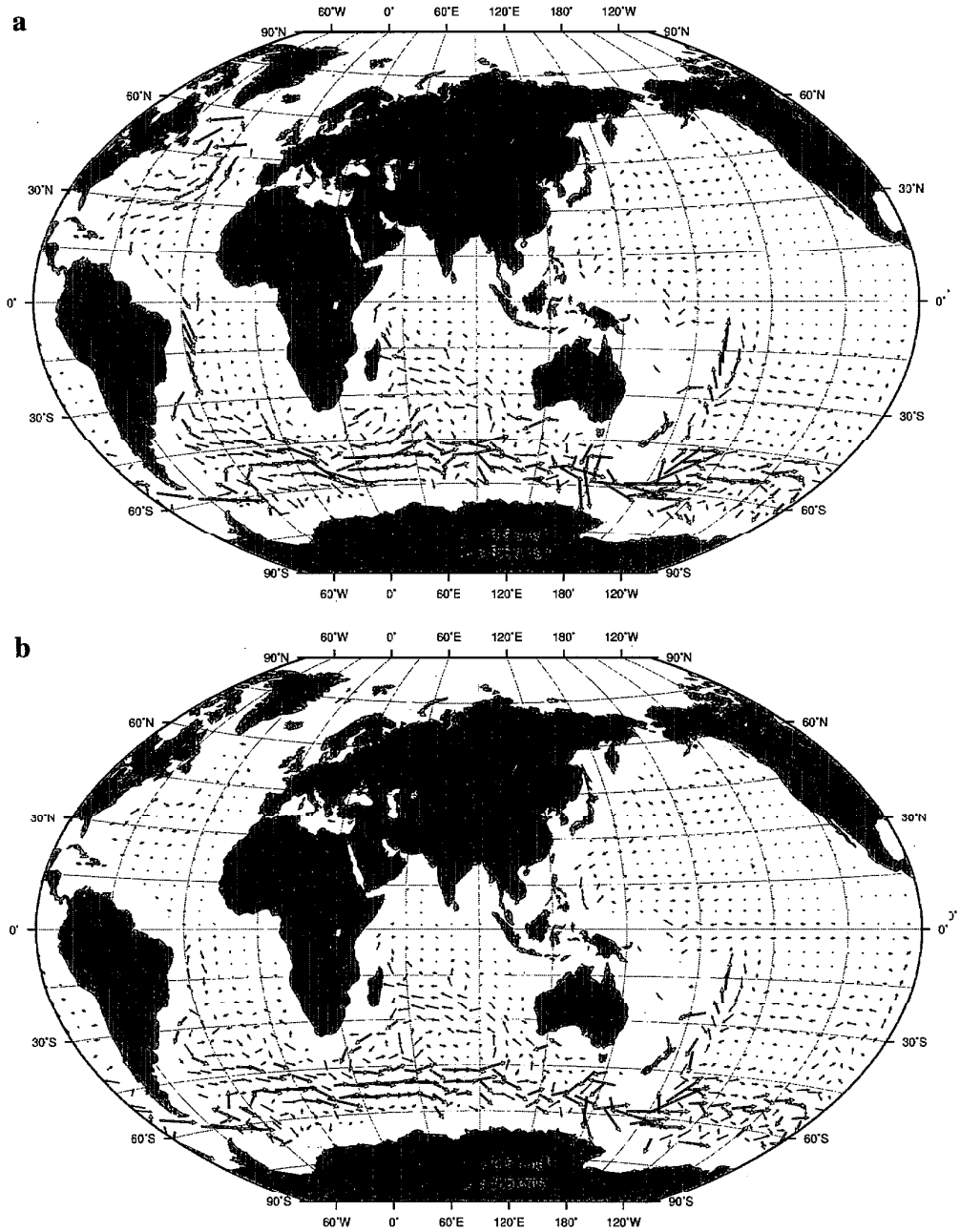

Figure 11. Velocity vectors (in cm s^{-1}) at 2.5 km: a) LGM (Exp. 3); MWE (Exp. 4).

eolian transport in the Arctic [*Pfirmann et al.*, 1989].

Western boundary currents off the American east coast are about 20 to 25% weaker in the LGM experiment than in present–day simulation. As a result, sedimentation rates differ by the same ratio in the western South Atlantic (Plate 1a, b).

The reduced sediment build–up along the Java Trench for the LGM simulation (in comparison to the PDC simulation) is the result of a 10–20% reduction of water transport from the Pacific Ocean via the Indonesian through flow into the Indian Ocean, as well as to a weakening of the South Indian Current [*Seidov and Haupt*, 1999].

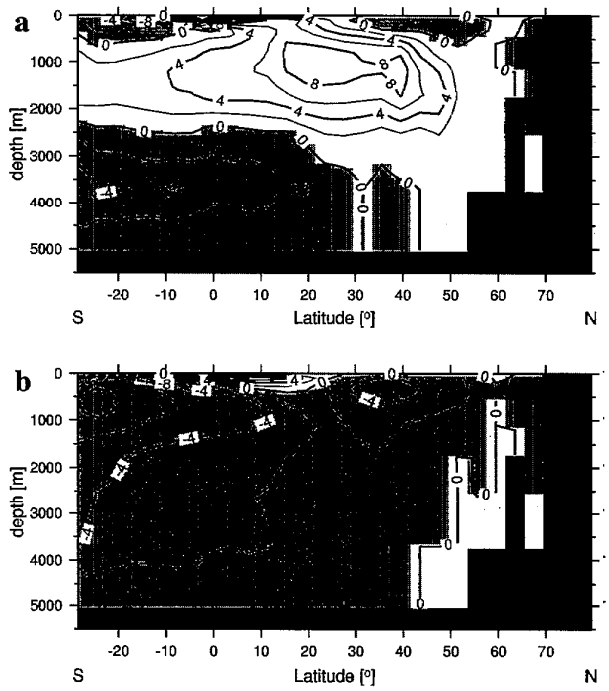

Figure 12. Meridional overturning in the Atlantic Ocean (in Sv; 1 Sverdrup (Sv) = 10^6 m^3s^{-1}): (a) LGM (Exp. 3) and (b) MWE (Exp. 4). The positive values depict clockwise motion while negative values (shaded) depict counterclockwise motion. The Atlantic overturning is valid only within this ocean's geographical boundary (with meridional walls at both sides; therefore the area south of 30°S is not shown).

Hollister and McCave [1984] describe the relation of deep-sea sediment accumulation to deep ocean storm intensity. Deep ocean storms are proportional to the intensity of the large-scale currents and mesoscale eddies. The change of the ACC strength in the past, as compared to today, gives a good example of the impact of a change in the intensity of the deep ocean circulation on sediment accumulation. The ACC is about 25% weaker than in the PDC experiment in our LGM run. The sediment accumulation over large areas beneath the ACC – south of the Crozet Plateau, east of the Kerguelen Plateau, in the Weddell Sea, on the southwestern side of the New Zealand Plateau, and in the Tasman Sea – is reduced by approximately the same percentage.

Interglacial sediment distribution. Northern meltwater events (Table 1) are easily traceable in sedimentation patterns. The freshwater impact of Heinrich events in the Nordic Seas and NNA includes the collapse of the conveyor (Figure 12b), leading to a totally different circulation in the NA in comparison to the PDC circulation regime. This applies to the upper as well to the deep ocean circulation, as shown in Figure 11b and Figure 14. Figure 12b implies that the thermohaline conveyor collapsed completely during the meltwater event (Figure 13). As a result, the cross–equatorial heat transport changed its sign. Almost the same amount of heat that was transported northward in the PDC experiment is now allocated to the SH. The dominance of NADW is replaced by dominance of AABW, and the southbound deep-ocean western boundary currents in the Atlantic Ocean were much weaker. Simulated sedimentation rates in the NA are now determined more closely by the eolian dust source, rather than by ocean currents (Plate 1c). In the absence of the southbound DWBC, the velocity vectors show a slow reversed northward water motion (Figure 11b and 14b). The collapse of the conveyor leads to a higher sedimentation rate around Iceland since sediment is not removed from southward flowing water masses (Plate 1c).

Meltwater sedimentation patterns around Antarctica look similar to those in the PDC and LGM runs. However, meltwater patterns show a further reduction of the LGM sedimentation rates, which, in turn, are already lower than the present–day rates. The sedimentation rate ratio MWE/PDC is close to the ratio of the water flows through the Drake Passage in these two runs. The same reduction ratio is found between the sedimentation rates and water transports across a vertical section between Australia and Antarctica. Sedimentation patterns in the Indian and Pacific Oceans, and in the seas around Australia and around New Zealand, are similar to those from our LGM simulation since the conveyor/circulation in those areas is much less affected by the collapse of the conveyor in the Atlantic Ocean (compare Figure 15a and b).

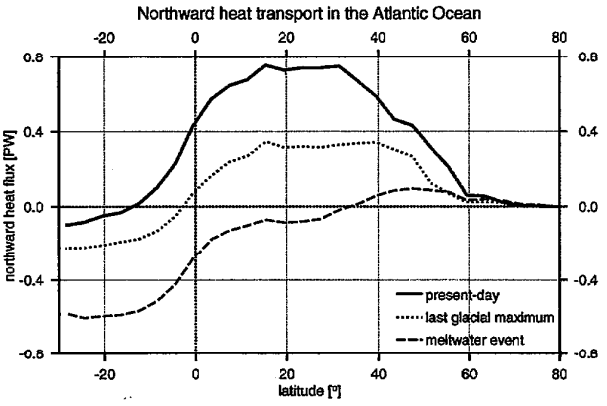

Figure 13. Northward heat transport in the Atlantic Ocean in present–day run (Exp. 2b), LGM run (Exp. 3), and MWE run (Exp. 4).

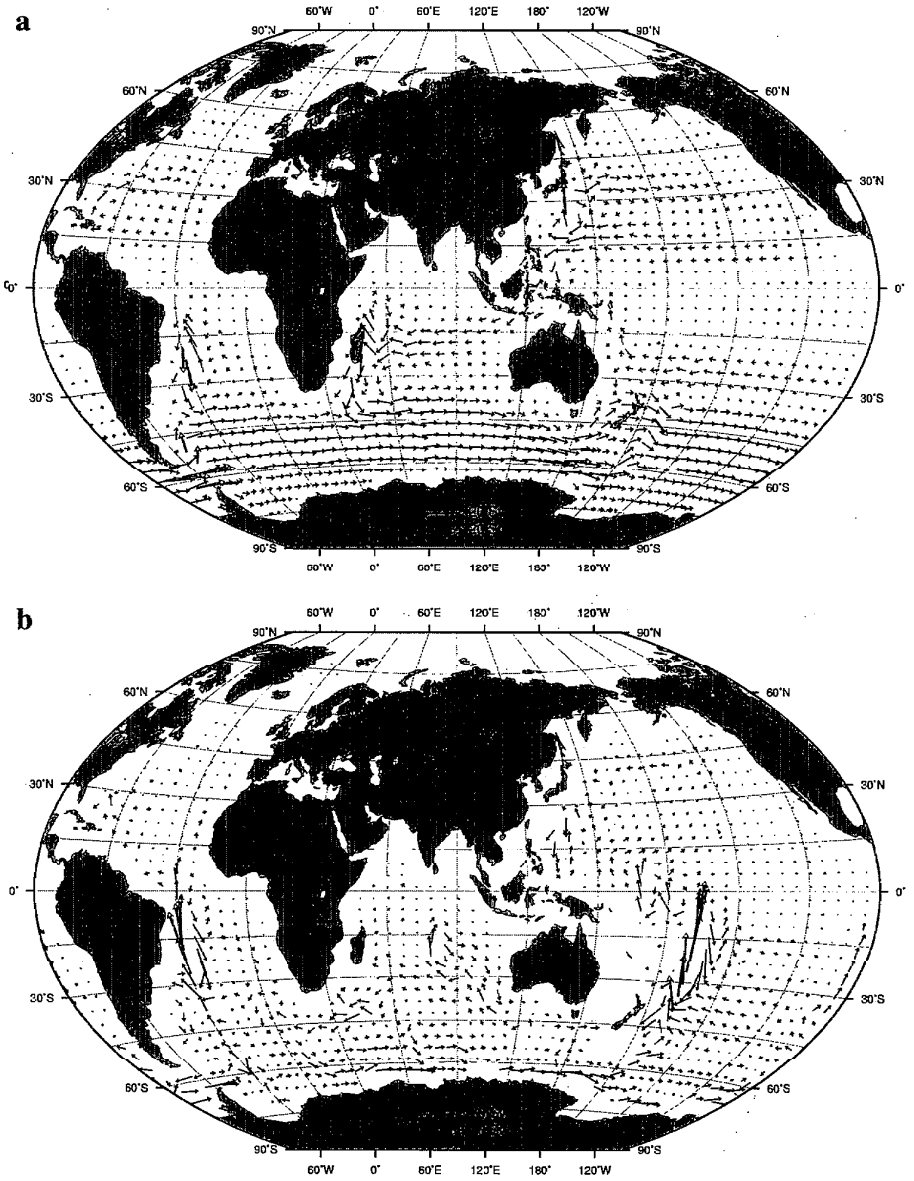

Figure 14. Total water mass transport for the MWE (Exp. 4) across vertical sections of the grid cells in Sv (1 Sverdrup (Sv) = 10^6 m^3s^{-1}): a) upper (above 1.5 km) ocean transport; b) deep (below 1.5 km) ocean transport. Note different scales of vectors for upper and deep ocean.

Sensitivity of global sedimentation to high–latitudinal surface density variations

In the four sensitivity experiments listed in Table 2, surface salinity in either the NNA, in the SO around the Antarctica, or in both locations was altered to simulate a decrease in sea surface density (Table 2; Figure 16). A more detailed description of the OGCM experiments is given in *Seidov et al.* [2001a] and *Seidov et al.* [2001b] (this volume). Note that salinity variation is just a convenient means of changing sea surface density in an OGCM. A 1 psu change of salinity would require about 5°C change of SST [*Pond and Pickard*, 1986]. Yet, an even smaller high–latitudinal warming may cause cryosphere melting, with a resulting freshwater input that would cause a far greater dilution of surface water. Therefore, we selected surface

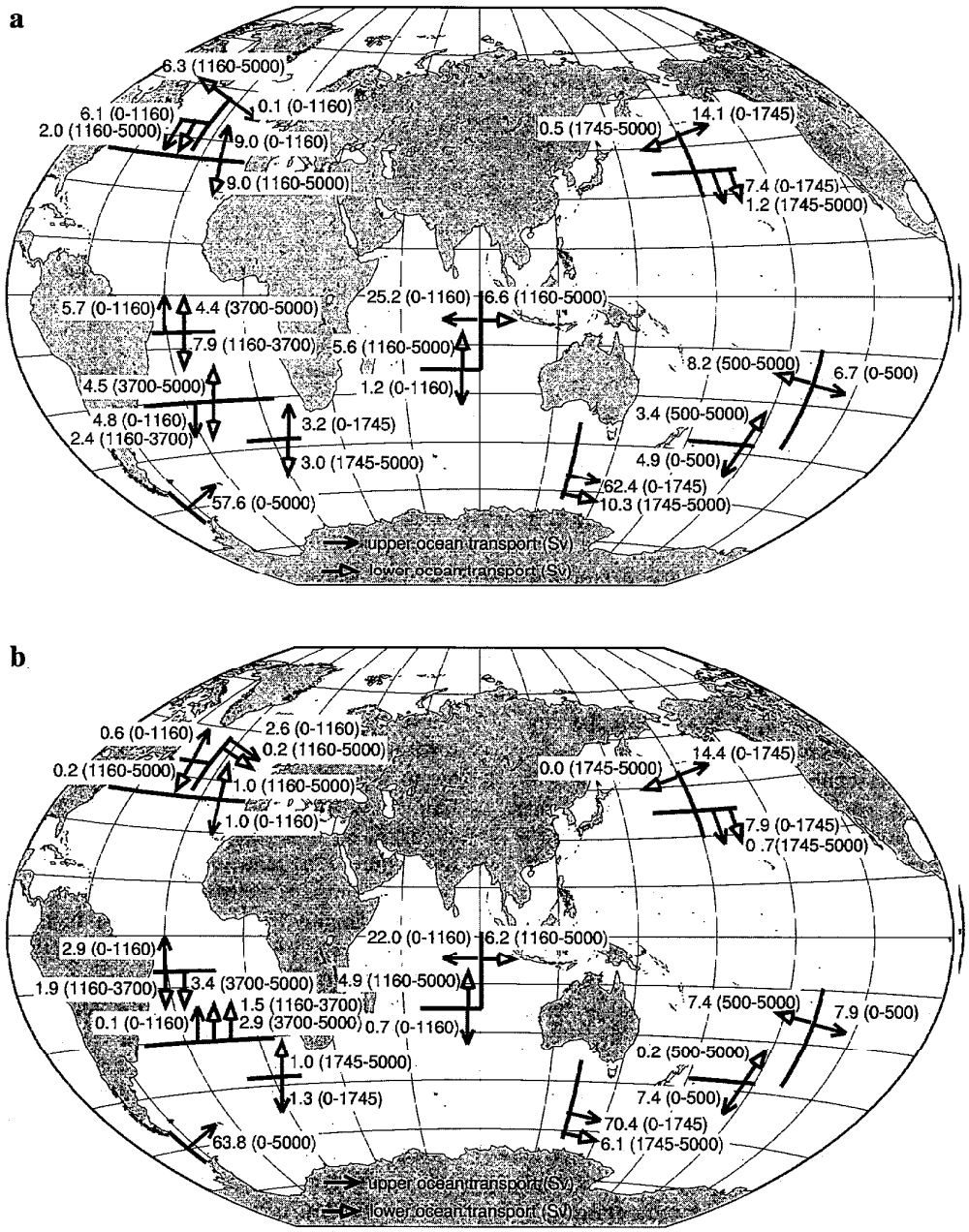

Figure 15. The water mass transport in Sv (1 Sverdrup (Sv) = 10^6 m^3s^{-1}) across chosen meridional and zonal vertical sections for different depths in different oceans: a) LGM (Exp. 3) and b) MWE (Exp. 4). Primarily, the transports in the upper and deep ocean are shown; in cases when upper and intermediate water movement essentially differs, the transports in three layers are shown to differentiate between the upper, intermediate–to–deep, and deep–to abyssal flows.

salinity as a far stronger and more realistic influence on surface water density.

The major implication of the sensitivity experiments is that a northern meltwater event results in a decreased NADW production and therefore an increased inflow of AABW into the NA, whereas during a southern meltwater event the NADW production is increased, as the AABW production weakens. In other words, an increase in the

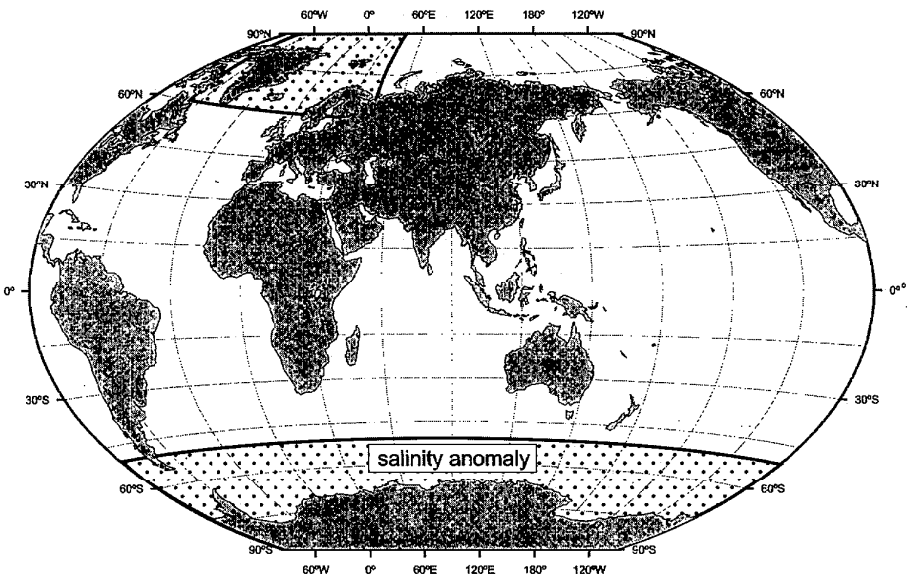

Figure 16. Idealized present–day meltwater events.

deepwater production in one hemisphere is equivalent to a reduction in the opposite hemisphere. A sketch of how the changed conveyor would look in the Atlantic is shown in Figure 3 in *Seidov et al.* [2001b] (this volume). To illustrate the concept of a seesaw character in the deepwater controls over the thermohaline conveyor, we reversed the signs of the salinity disturbances (that is, increased rather then decreased salinity in the same locations) in the SH (Exp. 8). As expected, this experiment produced circulation changes similar to those found in Exp. 5. However, there are important differences between the impacts in the SO and in the NA. All our experiments indicate that a smaller salinity change in the SO has a much stronger effect on the circulation than a stronger salinity change applied to the NA. Even in the run in which the salinity disturbance in the SO (-1 psu) was three times weaker than in the NA (-3 psu), the southern change overwhelmed the northern one.

As this work is a companion paper to Seidov et al., 2001b, we illustrate the changes of the circulation during the idealized northern and southern meltwater episodes by showing only water transports through specified sections (Figure 17). Meridional overturning for the Atlantic and global ocean can be found in *Seidov et al.* [2001b] (their Figures 5 and 6; this volume). All experiments (Table 2) demonstrate that the North Pacific is practically unaffected by salinity changes in either one or both hemispheres. This can be seen in both the OGCM calculations (Figure 17) and in sedimentation patterns from SEDLOB (Plate 2). In contrast, slowdown or speedup of the THC has a substantial effect on the sedimentation pattern in the Atlantic Ocean, in the western Indian Ocean, and around Antarctica.

The slowdown of the THC caused by a freshening of the surface water in the NNA (Exp. 5) has an effect comparable to a positive salinity anomaly in the SH (Exp. 8). In Exp. 5, the NA meridional overturning decreases from almost 20 Sv in the control run (Exp. 2b) (Figure 8b) to 6.6 Sv (Figure 17a), and to 5.9 Sv in Exp. 8 (Figure 17d). During a northern meltwater event intensified by a positive salinity anomaly in the SH (Exp. 6), meridional overturning shows only 2 Sv of deepwater production in the central North Atlantic (Figure 17b).

Exp. 7 illustrates that the thermohaline circulation in the Atlantic in its present–day mode can easily speed up in response to surface water freshening in the SO. Reduction in the surface density around Antarctica suppresses deepwater production and curtails northward AABW inflow. This allows more deepwater outflow from the Atlantic and hence stronger NADW production (~30 Sv) with a very strong DWBC (Figure 17c).

The NADW outflow across 30°S, transport in the Drake Passage, the East–Australian DWBC, cross-equatorial heat transport and maximum northward heat transport in the PDC for the four experiments from Table 2 are shown in Table 3. All overturning related parameters for the NA are proportional to the NADW production, whereas total transport through the Drake Passage and the global cross–equatorial heat transport are inversely proportional to the NADW production.

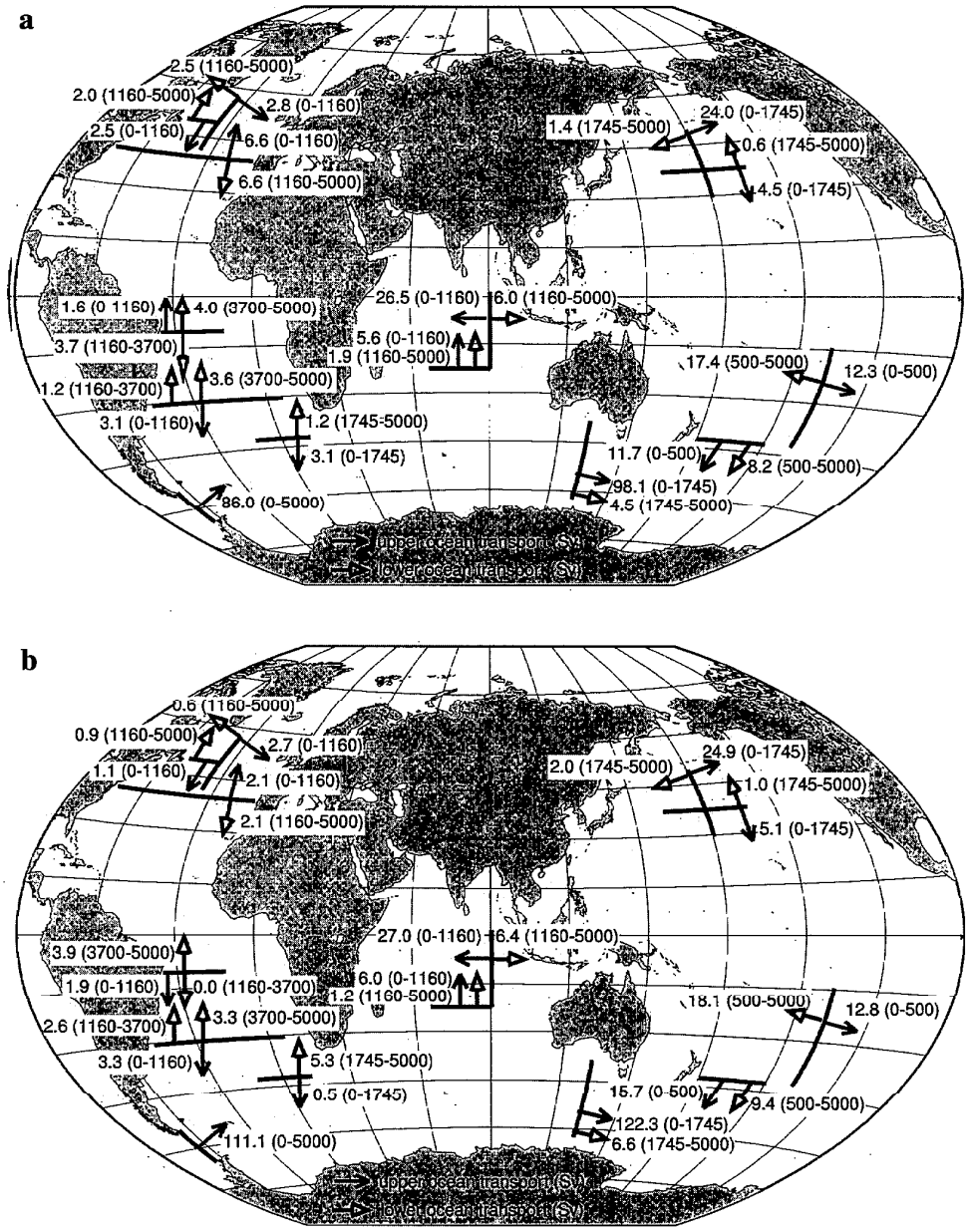

Figure 17. The water mass transport in Sv (1 Sverdrup (Sv) = 10^6 m^3s^{-1}) across chosen meridional and zonal vertical sections for different depths in different oceans: a) Exp. 5, b) Exp. 6, c) Exp. 7, and d) Exp. 8. Primarily, the transports in the upper and deep ocean are shown; in cases when upper and intermediate water movement essentially differs, the transports in three layers are shown to differentiate between the upper, intermediate–to–deep, and deep–to abyssal flows.

Sedimentation rate maps for these experiments (Plate 2b, 2a, 2d, 1a, and 2c; same order as the previously listed experiments) reveal that the strength of the DWBC in the western North Atlantic, especially in the Caribbean Sea, is the key governing factor for sedimentation rates under the DWBC and in adjacent areas. For other regions in the world ocean, it is not obvious that the circulation controls the accumulation. For instance, even substantial changes in

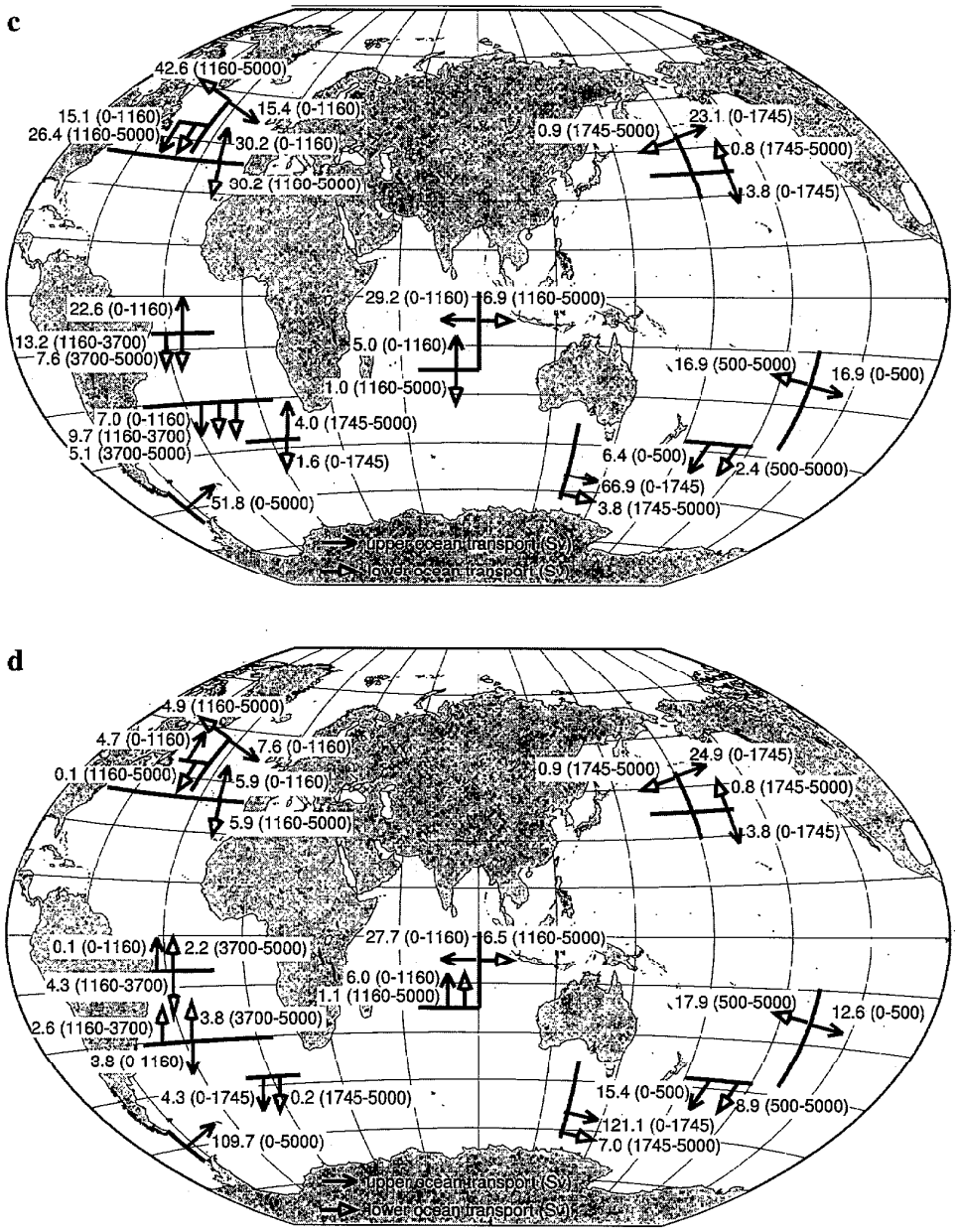

the THC do not noticeably affect the sedimentation pattern in the Pacific Ocean.

SUMMARY AND CONCLUSIONS

As ocean currents at least partially control sediment drifts, these drifts may be indicative of major changes in circulation patterns. We have performed numerical experiments designed to evaluate this idea. In these experiments, we pursued three goals: (1) The first group of the experiments is designed to identify the effect of different ocean model numerical mixing schemes on sedimentation patterns and sedimentation rates. To achieve this goal, we used two different surface sources of eolian dust, a highly idealized and a more realistic present–day global distribution. (2) The second set of experiments simulates the impact of different sea surface boundary conditions for different glacial–to–interglacial modes. This goal has been

Table 3. Results of present–day sensitivity experiments with different amplitudes of sea surface salinity anomalies in psu. Salinity anomalies are added to the present–day annual mean sea surface salinity in the bands between 60°N and 80°N in NA, in the lens at about 50°N in NNA, and band between 50°S and the coast of the Antarctica (SO). The modified salinity was merged using a cosine filter to the unchanged field within two latitudinal grid points (8°). In the SO the anomalies are circumglobal. All OGCM runs were performed with the Gent–McWilliams [1990] isopycnal mixing scheme.

Exp.	NA	SO	NADW production north of 30°S (Sv)	maximal northward heat transport (PW)	NA cross–equatorial heat transport (PW)	global cross–equatorial heat transport (PW)	water transport through Drake Passage (Sv)
#6	-3	+1	2.1	0.25	-0.1	-0.88	111.1
#8	–	+1	5.8	0.35	0.1	-0.74	109.7
#5	-3	–	6.5	0.4	0.15	-0.66	86.0
#2b	–	–	20.0	0.75	0.4	-0.38	81.6
7#	–	-1	30.2	1.0	0.75	0.01	51.8

NA – North Atlantic
SO – Southern Ocean
1 Sv = 10^6 m^3/s
1 PW = 10^{15} W

achieved through applying sea surface conditions from paleo–climatic reconstructions using the more realistic present–day eolian dust load in the lower atmosphere. (3) The third set of experiments is designed to test sensitivity of the global thermohaline conveyor and deep–sea sediment accumulation to changes of the sea–surface density in high latitudes, introduced as idealized meltwater events in the Northern and Southern Hemispheres. These runs assess the key issue of large–scale climatic changes and whether they can be unambiguously traced in coupled OGCM–sediment transport models. Thus, the results may tell us whether the sedimentologic record can be used to evaluate the impact of global warming through comparison with past meltwater and glacial cycles.

The link between millennial–scale changes in ocean currents and sedimentation is evident in our experiments and may enable model-data comparison, especially if sea surface sediment sources are better known. As a first step in this direction, we have modeled the LGM and a subsequent meltwater event characterized by substantial changes in the thermohaline ocean conveyor. The simulations suggest stronger dependence of the sediment drift patterns on the deep-ocean circulation regime rather than on currents in the upper and mid–depth ocean. Importantly, these experiments indicate that the geologic record of eolian dust accumulation can be used to trace and verify modeled circulation patterns, provided that the deep–ocean current system was substantially distinctive from other circulation modes (for example, LGM mode is different from the present–day mode, and MWE is strikingly different from both these two modes).

However, there are many limitations to our first–order, coarse resolution, modeling study. The coarseness of our resolution limits the results in many ways. All modeled currents except for the ACC are weaker than the observed currents, so our ability to model realistic sedimentation rates is limited as they are strongly linked to the strength of sea floor currents. However, we are able to reconstruct schematic patterns of changes in sediment accumulation in the regions known for high sediment deposition. Despite significant circulation changes, the results obtained from the sedimentation model for all three time slices, present–day, LGM, and MWE, show low sedimentation rates for the central Pacific Ocean [*Rea et al.*, 1985; *Lisitzin*, 1996]. The consistency of this pattern may enable the modeled paleocirculation to be verified against geologic record. This result could dramatically increase our confidence in modeling of past ocean climates.

For this first–order study, we were unable to compile global sea surface sources of eolian dust for the past, neither for the LGM nor the MWE. This must be viewed as a major task for future studies.

Importantly, several changes in the ocean model, including a slight imbalance in the northern–southern hemispheric asymmetry driven by warm ocean surface waters in the NNA, a moderately cool northern North Pacific, and much colder SO, appear to be traceable in the sediment transport model. The decrease in sea surface density in the SO and in the NNA lead to a "seesaw" effect, as envisioned by *Broecker* [1998, 2000] and *Stocker* [1998]. This seesaw effect was an issue in the recent numerical simulations done by *Seidov and Maslin* [2001] and *Seidov et al.* [2001a] that confirmed a flip–flop operation of the global conveyor. The seesaw effect implies that changes in the ocean conveyor mirror freshwater impacts, i.e., a response of the deep–ocean currents to an increase in the deep–water production in one hemisphere is equivalent to a decrease in the opposite hemisphere. In other words, simulations suggest that a decreased deep–water production caused by a de–densification in one hemisphere can be achieved by a densification of the high–latitudinal sea surface water in the opposite hemisphere. These changes of the thermohaline circulation appeared to be easily traceable in the alteration of sediment drifts, justifying the attempts to use sediment as a tracer of change of the ocean circulation through ages.

APPENDIX

Abbreviations and symbols	
AABW	=Antarctic Bottom Water
ACC	=Antarctic Circumpolar Current
DWBC	=deep western boundary current
FF	=form factor
GMMS	=Gent–McWilliams mixing scheme
IDWBC	=Indian Ocean deep western boundary current
LGM	=last glacial maximum
NA	=North Atlantic
NADW	=North Atlantic Deep Water
NNA	=northern North Atlantic
MOM	=modular ocean model
MWE	=meltwater event
OGCM	=ocean global circulation model
PDC	=present–day sea surface climatology
SEDLOB	=SEDimentation in Large Ocean Basins (sediment transport model)
SH	=Southern Hemisphere
SO	=Southern Ocean
SSS	=sea surface salinity
SST	=sea surface temperature
Sv	=Sverdrup (1 Sv = 10^6 m^3s^{-1})
SWP–DWBC	=Southwest Pacific deep western boundary current
THC	=thermohaline circulation
VAMS	='vertical adjustment' mixing scheme
γ	=porosity of sediment
ρ_s	=density of sediment

Acknowledgments. We thank the reviewers Jan Harff, Bill Hay, and John Tipper for their critical remarks that essentially improved the manuscript. This study is partly supported by National Science Foundation (grant #9975107 and ATM 00-00545).

REFERENCES

Allen, P.A., 1997, Earth surface processes. Blackwell Science, London, 404 pp.

Beckmann, A., 1998: The representation of bottom boundary layer processes in numerical ocean circulation models, In: E.P. Chassignet and J. Verron (Editors), *Ocean Modeling and Parameterization*. Kluwer, Boston, pp. 135-154.

Bitzer, K. and R. Pflug, 1990: DEPOD: A three-dimensional model for simulating clastic sedimentation and isostatic compensation in sedimentary basin, In: T.A. Cross (Editor), *Quantitative Dynamics Stratigraphy*. Prentice Hall, N.Y., pp. 335-348.

Bohrmann, G., R. Henrich and J. Thiede, 1990: Miocene to Quaternary paleoceanography in the northern North Atlantic: Variability in carbonate and biogenic opal accumulation, In: U. Bleil and J. Thiede (Editors), *Geological History of the Polar Oceans: Arctic versus Antarctic*. Kluwer Academic Publications, Norwell, Massachusetts, pp. 647-675.

Boyle, E.A. and L.D. Keigwin, 1987: North Atlantic thermohaline circulation during the past 20,000 years linked to high-latitude surface temperature, *Nature*, 330: 35-40.

Broecker, W., 1991: The great ocean conveyor, *Oceanography*, 1: 79-89.

Broecker, W.S., 1998: Paleocean circulation during the last deglaciation: A bipolar seesaw?, *Paleoceanography*, 13: 119-121.

Broecker, W.S., 2000: Was a change in thermohaline circulation responsible for the Little Ice Age?, *Proc. Nat. Acad. Sci.*, 97(4): 1339-1342.

Broecker, W.S. and G.H. Denton, 1989: The role of ocean atmosphere reorganizations in glacial cycles, *Geochimica Cosmochimica Acta*, 53: 2465-2501.

Bryan, K., 1969: A numerical method for the study of the circulation of the world ocean, *Journal of Computational Physics*, 4: 347-376.

Cao, S. and I. Lerche, 1994: A quantitative model of dynamical sediment deposition and erosion in three dimensions, *Computers & Geosciences*, 20: 635-663.

Carter, L. and J.S. Mitchell, 1987: Late Quaternary sediment pathways through the deep ocean, east of New Zealand, *Paleoceanography*, 2(4): 409.

Carter, R.M., L. Carter and I.N. McCave, 1996: Current controlled sediment deposition from the shelf to the deep ocean: The Cenozoic evolution of circulation through the SW Pacific gateway, *Geologische Rundschau*, 85: 438-451.

CLIMAP, 1981: Climate: Long-Range Investigation, Mapping, and Prediction (CLIMAP) Project Members, Seasonal reconstructions of the Earth's surface at the Last Glacial Maximum. *Map and Chart Ser. MC-36*. Geological Society of America, Boulder, Colorado, pp. 1-18.

Cox, M., 1984: A primitive equation, 3-dimensional model of the ocean, 1, Technical Report No. 1, 250 pp. Ocean Group, Geophys. Fluid Dyn. Lab., Princeton Univ., Princeton University, New Jersey.

Crowley, T. and K.-Y. Kim, 1992: Complementary roles of orbital insolation and north Atlantic deep water during late Pleistocene interglacials, *Paleoceanography*, 7: 521-528.

Dowling, L.M. and I.N. McCave, 1993: Sedimentation on the Feni drift and late glacial bottom water production in the northern Rockall Trough, *Sedimentary Geology*, 82: 79-87.

Ericksen, M.C., D.S. Masson, R. Slingerland and D. Swetland, 1989: Numerical simulation of circulation and sediment transport in the late Devonian Catskill Sea, In: T.A. Cross (Editor), *Quantitative Dynamic Stratigraphy*. Prentice Hall, Englewood Cliffs, pp. 295-305.

ETOPO5, 1986: Digital Relief of the Surface of the Earth,, National Geophysical Data Center, Boulder, Colorado.

Fairbanks, R.G., 1989: A 17,000-year glacio-eustatic sea level record: Influence of glacial melting rates on the Younger Dryas event and deep-ocean circulation, *Nature*, 342: 637-642.

Faugeres, J.C., M.L. Mezerais and D.A.V. Stow, 1993: Contourite drift types and their distribution in the North and South Atlantic Ocean basins, *Sedimentary Geology*, 82: 189-203.

Fichefet, T., S. Hovine and J.-C. Duplessy, 1994: A model study of the Atlantic thermohaline circulation during the Last Glacial Maximum, *Nature*, 372: 252-255.

Flood, R.D. and A.H. Shor, 1988: Mud waves in the Argentine Basin and their relationship to bottom circulation pattern, Part A, *Deep Sea Research*, 35: 943-971.

Ganopolski, A., S. Rahmstorf, V. Petoukhov and M. Claussen, 1998: Simulation of modern and glacial climates with a coupled global model of intermediate complexity, *Nature*, 391: 351-356.

Gent, P.R. and J.C. McWilliams, 1990: Isopycnal mixing in ocean circulation models, *Journal of Physical Oceanography*, 20: 150-155.

Goodman, P.J., 1998: The role of North Atlantic Deep Water formation in an OGCM's ventilation and thermohaline circulation, *J. Phys. Oceanogr.*, 28: 1759-1785.

Goosse, H. and T. Fichefet, 1999: Importance of ice-ocean interactions for the global ocean circulation: A model study, *Journal of Geophysical Research*, 104(C10): 23337-23355.

Granjeon, D. and P. Joseph, 1999: Concepts and applications of a 3D multiple lithology, diffusive model in stratigraphic modeling, In: J. Harbaugh, W.L. Watney, E.C. Rankey, R. Slingerland, R.H. Goldstein and E.K. Franseen (Editors), *Numerical Experiments in Stratigraphy: Recent Advances in Stratigraphy/Sedimentologic Computer Simulations. Special publication Series #62*. SEPM (Society for Sedimentary Geology)/Special Publication Series #62, Kansas, pp. 197-210.

Haupt, B.J., 1995: Numerische Modellierung der Sedimentation im nördlichen Nordatlantik, 54, Sonderforschungsbereich 313, Universität Kiel, Kiel.

Haupt, B.J., C. Schäfer-Neth and K. Stattegger, 1994: Modeling sediment drifts: A coupled oceanic circulation-sedimentation model of the northern North Atlantic, *Paleoceanography*, 9(6): 897-916.

Haupt, B.J., C. Schäfer-Neth and K. Stattegger, 1995: Three-dimensional numerical modeling of late Quaternary paleoceanography and sedimentation in the northern North Atlantic, *Geologische Rundschau*, 84: 137-150.

Haupt, B.J. and K. Stattegger, 1999: The ocean-sediment system and stratigraphic modeling in large basins, In: J. Harbaugh, W.L. Watney, E.C. Rankey, R. Slingerland, R.H. Goldstein and E.K. Franseen (Editors), *Numerical Experiments in Stratigraphy: Recent Advances in Stratigraphy/Sedimentologic Computer Simulations. Special publication Series #62*. SEPM (Society for Sedimentary Geology)/Special publication Series #62, Kansas, pp. 313-321.

Haupt, B.J., K. Stattegger and D. Seidov, 1999: SEDLOB and PATLOB: Two numerical tools for modeling climatically-forced sediment and water volume transport in large ocean basins, In: J. Harff, J. Lemke and K. Stattegger (Editors), *Computerized Modeling of Sedimentary Systems*. Springer, New York, pp. 115-147.

Hollister, C.D. and I.N. McCave, 1984: Sedimentation under deep-sea storms, *Nature*, 309: 220-225.

Honjo, S., 1990: Particle fluxes and modern sedimentation in the Polar Oceans, In: W.O. Smith (Editor), *Polar Oceanography, Part B*. Acad. Press, Boston, Massachusetts, pp. 687-739.

Honjo, S., 1996: Fluxes of particles to the interior of the open oceans, In: V. Ittekkot, P. Schäfer, S. Honjo and P.J. Depetris (Editors), *Particle Flux in the Ocean. SCOPE Report 57*. Chichester, Chichester, pp. 91-154.

Johnson, D.A. and J.E. Damuth, 1979: Deep thermohaline flow and current-controlled sedimentation in the Amirante Passage: Western Indian Ocean, *Marine Geology*, 33: 1-44.

Kolla, V., S. Eittreim, L. Sullivan, J.A. Kostecki and L.H. Burckle, 1980: Current-controlled, abyssal microtopography and sedimentation in Mozambique Basin, southwest Indian Ocean, *Marine Geology*, 34: 171-206.

Lehman, S.J.e.a., 1991: Initiation of Fennoscandina ice-sheet retreat during the last glaciation, *Nature*, 349: 513-516.

Lessenger, M. and I. Lerche, 1999: Inverse modeling, In: J. Harbaugh, W.L. Watney, E.C. Rankey, R. Slingerland, R.H. Goldstein and E.K. Franseen (Editors), *Numerical Experiments in Stratigraphy: Recent Advances in Stratigraphy/Sedimentologic Computer Simulations. Special publication Series #62*. SEPM (Society for Sedimentary Geology)/Special publication Series #62, Kansas, pp. 29-31.

Lisitzin, A.P., 1996, Oceanic sedimentation: lithology and geochemistry. American Geophysical Union, Washington, D.C., 400 pp.

Lorenz, S., B. Grieger, H. P. and K. Herterich, 1996: Investigating the sensivity of the atmospheric general circulation Model ECHAM 3 to paleoclimate boundary conditions., *Geol. Rundsch.*, 85: 513-524.

Maier-Reimer, E., U. Mikolajewicz and K. Hasselmann, 1991: On the sensitivity of the global ocean circulation to changes in the surface heat flux forcing, *Max-Plank-Institut für Meteorologie, Hamburg, Report No. 68*: 67.

Maier-Reimer, E., U. Mikolajewicz and K. Hasselmann, 1993: Mean circulation of the Hamburg LSG OGCM and its sensitivity to the thermohaline surface forcing, *Journal of Physical Oceanography*, 23: 731-757.

Manabe, S. and R. Stouffer, 1997: Coupled ocean-atmosphere model response to freshwater input: Comparison to Younger Dryas event, *Paleoceanography*, 12: 321-336.

Manabe, S. and R.J. Stouffer, 1988: Two stable equilibria of a coupled ocean-atmosphere model, *Journal of Climate*, 1: 841-866.

Manabe, S. and R.J. Stouffer, 1995: Simulation of abrupt change induced by freshwater input to the North Atlantic Ocean, *Nature*, 378: 165-167.

McCave, I.N. and B.E. Tucholke, 1986: Deep current controlled sedimentation in the western North Atlantic, In: P.R. Vogt and B.E. Tucholke (Editors), *The Geology of North America*. The Geological Society of America, Boulder, Colorado, pp. 451-468.

Mienert, J., J.T. Andrews and J.D. Milliman, 1992: The East Greenland continental margin (65°N) since the last deglaciation: Changes in seafloor properties and ocean circulation, *Marine Geology*, 106: 217-238.

Miller, M.C., I.N. McCave and P.D. Komar, 1977: Threshold of sedimentation under unidirectional currents, *Sedimentology*, 24: 507-528.

MOM-2, 1996: Documentation, User's Guide and Reference Manual (edited by R. C. Pacanowski), GFDL Ocean Technical

Report No. 3.2, Geophysical Fluid Dynamics Laboratory/NOAA, Princeton, N.J.

Nittrouer, C.A. and L.D. Wright, 1994: Transport of particles across continental shelves, *Review of Geophysics*, 32(1): 85-113.

Pacanowski, R., K. Dixon and A. Rosati, 1993: The GFDL Modular Ocean Users Guide, Geophys. Fluid Dyn. Lab., Princeton Univ., Princeton, N. J.

Pacanowski, R.C., 1996: MOM 2. Documentation, User's Guide and Reference Manual, GFDL Ocean Technical Report #3.2 edited by R. C. Pacanowski, Geophysical Fluid Dynamics Laboratory/NOAA, Princeton, N.J.

Paola, C., P.L. Heller and C.L. Angevine, 1992: The large scale dynamics of grain–size variation in alluvial basins, 1: Theory, *Basin Research*, 4: 73–90.

Pfirmann, S., I. Wollenburg, J. Thiede and M.A. Lange, 1989: Lithogenic sediment on Arctic pack ice: Potential aeolian flux and contribution to deep sea sediments, In: M. Leinen and M. Sarnthein (Editors), *Paleoclimatology and Paleometeorology: Modern and Past Patterns of Global Atmospheric Transport*. Kluwer Academic Publishers, New York, pp. 463-493.

Pond, S. and G.L. Pickard, 1986, Introductory Dynamical Oceanography. Pergamon Press, Oxford, UK, 329 pp.

Prospero, J.M., 1996: The atmospheric transport of particles to the ocean, In: V. Ittekkot, P. Schäfer, S. Honjo and P.J. Depetris (Editors), *Particle Flux in the Ocean. SCOPE Report 57*. John Wiley & Sons, Chichester, pp. 19-52.

Prospero, J.M., K. Barrett, T. Church, F. Dentener, R.A. Duce, H. Galloway, I.I. Lewy, J. Moody and P. Quinn, 1996: Atmospheric deposition of nutrients to the North Atlantic Basin, *Biogeochemistry*, 35: 27-37.

Rahmstorf, S., 1994: Rapid climate transitions in a coupled ocean-atmosphere model, *Nature*, 372: 82-85.

Rahmstorf, S., 1995a: Bifurcations of the Atlantic thermohaline circulation in response to changes in the hydrological cycle, *Nature*, 378: 145-149.

Rahmstorf, S., 1995b: Climate drift in an ocean model coupled to a simple, perfectly matched atmosphere, *Climate Dynamics*, 11: 447-458.

Rahmstorf, S. and M.H. England, 1997: Influence of Southern Hemisphere winds on North Atlantic Deep Water flow, *Journal of Physical Oceanography*, 27: 2040-2054.

Ram, M. and G. Koenig, 1997: Continous dust concentration profile of pre-Holocene ice from the Greenland Ice Sheet Project 2 ice core: Dust stadials, interstadials, and the Emian, *Journal of Geophysical Research*, 102(C12): 26641-26648.

Rea, D.K., 1994: The paleoclimatic record provided by eolian deposition in the deep sea: The geologic history of wind, *Review of Geophysics*, 32(1): 159-195.

Rea, D.K., M. Leinen and T.R. Janecek, 1985: Geologic approach to the long-term history of atmospheric circulation, *Science*, 227: 721-725.

Rebesco, M., R.D. Larter, P.F. Barker, A. Camerlenghi and L.E. Vanneste, 1994: The history of sedimentation on the continental rise west of the Antarctic Peninsula, *Terra Antarctica*, 1(2): 277-279.

Robinson, S.G. and I.N. McCave, 1994: Orbital forcing of bottom-current enhanced sedimentation on Feni Drift, NE Atlantic, during the mid-Pleistocene, *Paleoceanography*, 9(6): 943-972.

Ruddiman, W.F. and A. McIntyre, 1981: The mode and mechanism of the last deglaciation: Oceanic evidence., *Quaternary Research*, 16: 125-134.

Sarnthein, M., K. Winn, S.J.A. Jung, J.C. Duplessy, L. Labeyrie, H. Erlenkeuser and G. Ganssen, 1994: Changes in east Atlantic deepwater circulation over the last 30,000 years: Eight Time Slice Reconstructions, *Paleoceanography*, 9: 209-267.

Schmitz, W.J., Jr., 1995: On the interbasin-scale thermohaline circulation, *Reviews of Geophysics*, 33: 151-173.

Scott, J.R., J. Marotzke and P.E. Stone, 1999: Interhemispheric thermohaline circulation in a coupled box model, *Journal of Physical Oceanography*, 29: 351-365.

Seidov, D., E.J. Barron and B.J. Haupt, 2001a: Meltwater and the global ocean conveyor: Northern versus southern connections, *Global and Planetary Change*, in press.

Seidov, D. and B.J. Haupt, 1997a: Global ocean thermohaline conveyor at present and in the late Quaternary, *Geophysical Research Letters*, 24: 2817-2820.

Seidov, D. and B.J. Haupt, 1997b: Simulated ocean circulation and sediment transport in the North Atlantic during the Last Glacial Maximum and today, *Paleoceanography*, 12: 281-306.

Seidov, D. and B.J. Haupt, 1999: Last glacial and meltwater interbasin water exchanges and sedimentation in the world ocean, *Paleoceanography*, 14: 760-769.

Seidov, D., B.J. Haupt, E.J. Barron and M. Maslin, 2001b: Ocean bi-polar seesaw and climate: Southern versus northern meltwater impacts, *Geophysical Monograph (This Volume)*, D. Seidov, B.J. Haupt and M. Maslin (Editors), American Geophysical Union, Washington, D.C.

Seidov, D. and M. Maslin, 1999: North Atlantic Deep Water circulation collapse during the Heinrich events, *Geology*, 27: 23-26.

Seidov, D. and M. Maslin, 2001: Atlantic Ocean heat piracy and the bi-polar climate sea-saw during Heinrich and Dansgaard-Oeschger events, *Journal of Quaternary Science*, 16: in press.

Seidov, D., M. Sarnthein, K. Stattegger, R. Prien and M. Weinelt, 1996: North Atlantic ocean circulation during the Last Glacial Maximum and subsequent meltwater event: A numerical model, *Journal of Geophysical Research*, 101: 16305-16332.

Shanks, A.L. and J.D. Trent, 1980: Marine snow: Sinking rates and potential role in vertical flux, *Deep Sea Research*, 27, Part A: 137-143.

Shinn, E.A., G.W. Smith and J.M. Prospero, 2000: African dust and the demise of Caribbean coral reefs, *Geophysical Research Letters*, 27(19): 3029-3032.

Slingerland, R., J.W. Harbaugh and K.P. Furlong, 1994, Simulating Clastic Sedimentary Basins. PTR Prentice Hall, Englewood Cliffs, 220 pp.

Stattegger, K., B.J. Haupt, C. Schäfer-Neth and D. Seidov, 1997: Numerische Modellierung des Ozean–Sediment-Systems in großen Meeresbecken: Das Spätquartär im nördlichen Nordatlantik, *Geowissenschaften*, 15(1): 10-15.

Stocker, T.F., 1998: The seesaw effect, *Science*, 282: 61-62.

Stoessel, A., S.-J. Kim and S.S. Drijfhout, 1998: The impact of Southern Ocean sea ice in global ocean model, *J. Phys. Oceanogr.*, 28: 1999-2018.

Stommel, H., 1958: The abyssal circulation, *Deep-Sea Research*, 5: 80-82.

Sündermann, J. and R. Klöcker, 1983: Sediment transport modeling with applications to the North Sea, In: J. Sünderman and W. Lenz (Editors), *North Sea Dynamics*. Springer-Verlag, New York, pp. 453-471.

Syvitski, J.P.M. and S. Daughney, 1992: Delta2: Delta progradation and basin filling, *Computer and Geosciences*, 18(7): 839-897.

Tetzlaff, D.N. and J.W. Harbaugh, 1989, Simulating Clastic Sedimentation. Van Nostrand Reinhold, New York, 202 pp.

Toggweiler, J.R., K. Dixon and K. Bryan, 1989: Simulations of radiocarbon in a coarse-resolution world ocean circulation model, 1, Steady state prebomb distribution, *Journal of Geophysical Research*, 94: 8217-8242.

Toggweiler, J.R. and B. Samuels, 1995: Effect of Drake Passage on the global thermohaline circulation, *Deep Sea Research*, 42: 477-500.

Wang, X., P. Stone and J. Marotzke, 1999: Global thermohaline circulation. Part I. Sensitivity to atmospheric moisture transport, *J. Climate*, 12: 71-82.

Weaver, A.J., J. Marotzke, P.F. Cummins and E.S. Sarachik, 1993: Stability and variability of the thermohaline circulation, *Journal of Physical Oceanography*, 23: 39-60.

Zanke, U., 1982, Grundlagen der Sedimentbewegung. Springer–Verlag, Berlin, Heidelberg, New York, 402 pp.

E.J. Barron, EMS Environment Institute, Pennsylvania State University, University Park, PA 16802. (eric@essc.psu.edu)

B.J. Haupt, EMS Environment Institute, Pennsylvania State University, University Park, PA 16802. (bjhaupt@essc.psu.edu)

D.Seidov, EMS Environment Institute, Pennsylvania State University, University Park, PA 16802. (dseidov@essc.psu.edu)